THE UNIVERSITY OF OKLAHOMA

GRADUATE COLLEGE

ELECTRON EXCITATION OF THE FIRST POSITIVE BANDS OF N_2 AND OF THE FIRST NEGATIVE AND MEINEL BANDS OF N_2^+

A DISSERTATION

SUBMITTED TO THE GRADUATE FACULTY

in partial fulfillment of the requirements for the

degree of

DOCTOR OF PHILOSOPHY

BY

PAUL NELSON STANTON

Norman, Oklahoma

1968

ELECTRON EXCITATION OF THE FIRST POSITIVE BANDS OF N_2 AND OF THE FIRST NEGATIVE AND MEINEL BANDS OF N_2^+

APPROVED

Robert M. St. John

C C Lin

J M Canfield

S. E. Bahn, Jr.

Earl Larson

DISSERTATION COMMITTEE

ACKNOWLEDGEMENTS

The subject of this study was suggested by Dr. Robert M. St. John. The author is grateful for Dr. St. John's help and support during the research and writing of this report.

The author also wishes to thank Dr. John D. Jobe, Francis A. Sharpton, and James D. Walker, Jr. for their help in the construction of equipment and for their discussions and suggestions.

Financial support from September, 1965, through August, 1968, was provided by the National Aeronautics and Space Administration under the Graduate Traineeship program.

Particular thanks go to the author's wife, Susan, for her encouragement and help in writing this paper.

TABLE OF CONTENTS

		Page
LIST OF TABLES		vi
LIST OF ILLUSTRATIONS		vii
Chapter		
I.	INTRODUCTION	1
	Previous Work	1
	This Work	3
	Theory and Definitions	5
II.	EXPERIMENTAL APPARATUS	10
	Vacuum System	10
	Optical and Electronic System	12
	Electron Gun	15
III.	MEASUREMENT OF EXPERIMENTAL PARAMETERS	22
	Ground State Density	22
	Standardization	26
IV.	FIRST POSITIVE SYSTEM	36
	Relative Excitation Functions	39
	Absolute Effective Cross Sections	47
	Apparent Cross Sections	53
	Total Apparent Cross Section of $B^3\pi_g$ State	53
	Comparison of Experimental and Calculated Relative Cross Sections	56
	Comparison with Other Investigators	58
V.	FIRST NEGATIVE AND MEINEL BAND SYSTEMS OF N_2^+	59
	First Negative System	59
	Meinel Band System	65

TABLE OF CONTENTS (Cont'd.)

	Page
VI. CONCLUSION	69
LIST OF REFERENCES	73

LIST OF TABLES

Table		Page
1.	Effective Cross Sections of First Positive Bands	48
2.	Apparent Cross Sections of the Vibrational States of the N_2 $B^3\pi_g$ Electronic State	54
3.	Comparison of Relative Values of First Positive Effective Cross Sections with Calculated Transition Probabilities	57
4.	Effective Cross Sections of N_2^+ First Negative Bands	62
5.	Apparent Cross Sections of Vibrational States of the N_2^+ $B^2\Sigma_u^+$ Electronic State	62
6.	Effective Cross Sections of N_2^+ Meinel Bands	67
7.	Apparent Cross Sections of Vibrational States of the N_2^+ $A^2\pi_u$ Electronic State	67

LIST OF ILLUSTRATIONS

Figure		Page
1.	The Vacuum System	11
2.	Arrangement of Optical and Electronic Apparatus	13
3.	Electron Gun	16
4.	Schematic Diagram of Electronic Beam Chopper	18
5.	Energy Spread of Electron Beam	20
6.	Variation of I_P/I_BP with Time after Turning on Electron Gun	24
7.	Two Arrangements for Standardization	31
8.	Partial Energy Level Diagram of Molecular Nitrogen	37
9.	Variation of I_P with Distance of Region of Observation From Center of Electron Beam	40
10.	Relative Excitation Functions of N_2 First Positive Bands with v' = 0 through 5	42
11.	Relative Excitation Functions of N_2 First Positive Bands with v' = 6 through 9	43
12.	First Positive Excitation Functions at Threshold, v' = 2 through 7	45
13.	First Positive Excitation Functions at Threshold, v' = 8 through 12	46

LIST OF ILLUSTRATIONS (Cont'd.)

Figure		Page
14.	Scan of N_2 Spectrum from 5700 Å to 6200 Å	49
15.	Apparent Excitation Cross Sections of the $B^3\pi_g$ and $C^3\pi_u$ Electronic States of N_2	55
16.	Relative Excitation Functions of the (0,0) and (1,0) N_2^+ First Negative Bands.	60
17.	Apparent Cross Section of N_2^+ $B^2\Sigma_u^+$ Electronic State and Effective Cross Section of (0,0) First Negative Band.	64
18.	Relative Excitation Functions of the (3,0) and (4,1) N_2^+ Meinel Bands.	66

ELECTRON EXCITATION OF THE FIRST POSITIVE BANDS OF N_2 AND OF THE FIRST NEGATIVE AND MEINEL BANDS OF N_2^+

CHAPTER I

INTRODUCTION

Atomic and molecular collision processes have been of continual interest to astronomers and astrophysicists. Recent activity in upper atmospheric, space, and plasma physics has further stimulated the research in collision phenomena. Because of nitrogen's abundance in the earth's atmosphere, electron collision cross sections for nitrogen are of particular interest in explaining such natural occurrences as the Aurora, the air-glow, and lightening.

With many non-overlapping or only partially overlapping bands, the rich spectrum of nitrogen also makes it an ideal gas for studying many of the properties of diatomic molecules. Since nitrogen is chemically inert, it is easier to work within the laboratory than most other molecular gases.

Previous Work

The electron excitation of N_2 was studied as early as 1925 by D. C. Duncan.[1] In 1934, G. O. Langstroth recorded the relative excitation functions for N_2^+ first negative bands and N_2 second positive

bands at low electron energies. He showed that the relative intensities of different bands in the same band system were constant as a function of electron energy except at near onset.[2] S. E. Williams (1935) measured the absolute effective cross section of the group of first positive bands centered at 6500 Å and of the group at 5900 Å.[3] He then approximated the apparent cross section of the $B^3\pi_g$ state of N_2 by estimating the fraction of photons emitted in each group of bands. In 1937, F. P. Bundy obtained the relative excitation function of the N_2^+ bands at 3914 Å and 4278 Å.[4] The early investigators used photographic plates for measuring their relative intensities.

Recently (1955), D. T. Stewart measured the relative excitation functions of the (2,0) and (3,1) Meinel bands of N_2^+ and of the (2,0) first positive band of N_2.[5] In 1958, Stewart and E. Gabathuler measured the absolute effective cross sections of 10 N_2 second positive bands and also gave the excitation function for the bands.[6] Von E. Fink and K. H. Welge (1964) measured the relative excitation functions of the $N_2(C^3\pi_u)$ state and the $N_2^+(B^2\Sigma_u^+)$ state.[7] Absolute effective cross sections for 23 second positive bands were measured by John Jobe, Francis Sharpton, and Robert M. St. John in 1966.[8] The following workers have measured the absolute excitation functions of N_2^+ first negative bands: Stewart (1956)[9], W. F. Sheridan, O. Oldenberg, and N. P. Carleton (1961)[10], H. Nishimura (1968)[11], J. W. McConkey, J. M. Woolsey, and O. J. Burns (1967)[12], and R. Holland[12]. In Russia, V. V. Skubenich and I. P. Zapesochny have measured the absolute excitation cross sections for the bands of the

first positive, second positive, and fourth positive band systems of N_2 and for bands of the first negative and Meinel band systems of N_2^+.[13] They have published only absolute cross sections for the electronic states, $B^3\pi_g$, $C^3\pi_u$, and $D^3\Sigma_u^+$ of N_2 and the $B^2\Sigma_u^+$ and $A^2\pi_u$ of N_2^+ and have not given the individual cross sections for each band. B. N. Srivastava and I. M. Mirza (1968) measured the absolute cross sections for the electron excitation of the (0,0) first negative and (4,1) Meinel bands of N_2^+.[14] Except for Stewart in his 1955 work, the recent investicators used photomultipliers for measuring light intensities.

This Work

In this work absolute effective cross sections for the excitation of ground state ($X^1\Sigma_g^+$) N_2 by electron impact have been measured for 39 N_2 first positive bands ($B^3\pi_g$ - $A^3\Sigma_u^+$), 12 N_2^+ first negative bands ($B^2\Sigma_u^+$ - $X^2\Sigma_g^+$), and 10 N_2^+ Meinel bands ($A^2\pi_u$ - $X^2\Sigma_g^+$). The experimental apparatus and techniques used to measure the absolute effective cross sections and to record the effective excitation functions of the bands are described in this report. Results of the measurements are given.

The effective excitation functions from 0 - 50 eV are presented for first positive bands with v' values from 0 through 9. The curves exhibit two sharp peaks at 10 - 12 eV and at 14 - 15 eV. The second peak is caused by cascade from the second positive system ($C^3\pi_u$-$B^3\pi_g$) and decreases in height as v' increases. The first peak is primarily the result of direct electron excitation. The absolute effective cross

sections at the first peak in the excitation functions are listed for 39 first positive bands. The threshold of the excitation functions of bands with v' = 2 through 12 are plotted on an expanded energy scale to exhibit an S - shaped change of slope in the excitation functions about midway between onset and the maximum of the first sharp peak. Relative values of effective cross sections of bands with the same v' are compared with the corresponding relative values calculated from Franck-Condon factors.

Apparent excitation cross sections were calculated for the first 13 vibrational states of the $B^3\pi_g$ electronic state, and the results are listed. The total apparent excitation function from 0 - 50 eV for the $B^3\pi_g$ electronic state, obtained by summing the apparent cross sections of the vibrational states, is shown. The maximum of the first peak in the apparent excitation function occurred at 11 eV and had a value of 62×10^{-18} cm^2; the maximum of the second peak occurred at 14.5 eV and had a value of 85×10^{-18} cm^2.

Excitation functions for the (0,0) and (1,0) N_2^+ first negative bands are given. The absolute effective cross sections of 12 first negative bands were measured at 120 eV, the position of the maximum in the excitation functions, and the results are listed. The value obtained for the (0,0) band was 15.6×10^{-18} cm^2. Apparent excitation cross sections were calculated for the first four vibrational states of the N_2^+ $B^2\Sigma_u^+$ electronic state, and the results are shown. The measurements of this work are compared with those of previous investigations.

Effective excitation functions for the (3,0) and (4,1) N_2^+ Meinel bands are shown. The results of the measurements of the maximum values of the absolute effective cross sections for 10 Meinel bands at 100 eV are listed. Apparent cross sections calculated for the first 6 vibrational states of the N_2^+ $A^2\pi_u$ electronic state at 100 eV are given, and their sum was found to be 47×10^{-18} cm^2.

The estimated accuracy of the measured absolute effective electron excitation cross sections for most of the bands observed was 20 per cent.

Theory and Definitions

The collisions that an electron suffers when passing through a target gas may be divided into two categories, elastic collisions and inelastic collisions. In elastic collisions, the relative kinetic energy of the colliding particles is conserved, and because of the great difference in the masses of electrons and molecules, the electron undergoes little change in its energy. Only its direction of motion is altered.

In inelastic collisions, part of the relative kinetic energy is converted to internal energy of the molecule or is used for the removal of an electron from the molecule. Often both processes occur during a collision. Different types of inelastic collisions may be distinguished by observing the states of the molecules after the collisions. For example, collisions of electrons with ground state $X^1\Sigma_g^+$ of N_2 which leave the molecule in the state of $B^3\pi_g$ may be distinguished from collisions which leave the molecule in the state of $C^3\pi_u$.

When an electron with a velocity v passes through a gas, there exists a certain probability, dP, that the electron will undergo a collision in the distance dx. For a uniform gas, this probability will be constant along the path of the electron. Assume for a moment that gas molecules are hard spheres of cross sectional area σ and number density N, and that the electrons are point projectiles. If an electron beam of cross sectional area A is passed through the gas along the direction x, then the total target area presented to the electrons in a small volume element, Adx, is given by σNAdx, where no target in Adx shields another from the electrons when the gas density is low. The probability of a collision between an electron and a gas molecule in dx is given by the total target area divided by the total area:

$$dP = \frac{\sigma NAdx}{A} \quad . \tag{1}$$

Using the hard sphere concept of cross section and Eq. (1), a cross section Q(j) for the excitation of the jth state by electron impact with the ground state is now defined as

$$Q(j) = \frac{1}{N(g)} \frac{dP(j)}{dx} \quad , \tag{2}$$

where N(g) is the number density of ground state molecules and dP(j) is the probability that an electron will excite the jth state in distance dx. The jth level can also be populated by radiative transitions from states with higher energy (cascade in), by photon excitation (imprisonment of resonance radiation), and by nonradiative transfer of energy in

collisions of excited molecules with electrons, ground state molecules, or other excited molecules. Depopulating mechanisms include spontaneous emission of radiation (cascade out), stimulated emission of radiation, and collisions with ground state molecules, excited molecules, electrons, and the walls of the collision chamber.

The lifetimes of excited states with allowed radiative transitions are usually so short that most of the states do not diffuse far from the electron beam, thus making collisions with the chamber walls negligible. When the electron current density and molecular density are low, the mechanisms other than direct electron excitation and cascade also become negligible. Assuming that only direct electron excitation and cascade need be considered, the steady state population equation of the jth level is given by

$$\text{direct electron excitation} + \text{cascade in} = \text{cascade out} \qquad (3)$$

The rate of populating the jth level by direct electron excitation per unit volume is given by

$$\frac{J}{e} N(g)Q(j) \ ,$$

where J is the electron current density and e is the charge on an electron. The electrons are assumed to be monoenergetic. The rates of cascade in and cascade out of the jth state are given by

$$\sum_{i>j} A(i,j)N(i) \quad \text{and} \quad \sum_{k<j} A(j,k)N(j) \ ,$$

where A(i,j) and A(j,k) are the probabilities per second of transitions from i to j and from j to k. N(i) and N(j) are the number densities of the ith and the jth states. Thus, the steady state population Eq. (3) can be written as

$$\frac{J}{e} N(g)Q(j) + \sum_{i>j} A(i,j)N(i) = \sum_{k<j} A(j,k)N(j) \quad . \tag{4}$$

Integrating each term of Eq. (4) over a plane perpendicular to the electron beam gives the population equation per unit length of the beam. The first term of the equation becomes

$$\int \frac{J}{e} N(g)Q(j)ds = \frac{I_B}{e} N(g)Q(j) \quad , \tag{5}$$

where I_B is simply the electron beam current. Solving the population equation for Q(j) now gives

$$Q(j) = \sum_{k<j} \frac{e}{I_B N(g)} \int A(j,k)N(j)ds - \sum_{i>j} \frac{e}{I_B N(g)} \int A(i,j)N(i)ds. \tag{6}$$

A quantity which is often used in analyzing the experimental data is defined as

$$Q(j,k) = \frac{e}{I_B N(g)} \int A(j,k)N(j)ds \quad , \tag{7}$$

and is called the effective cross section for excitation of the j to k transition. The equation for Q(j) now can be written as

$$Q(j) = \sum_{k<j} Q(j,k) - \sum_{i>j} Q(i,j) \quad . \tag{8}$$

Thus Q(j) equals the sum of the effective cross sections for transitions out of the jth level minus the sum of the effective cross sections for transitions into the jth level.

The effective cross section Q(j,k) may be expressed in terms of experimentally measurable quantities since $\int A(j,k)N(j)ds$ is the number of photons per second per unit path length of the beam emitted in the j to k transition. The variation of Q(j,k) with electron energy is called the optical excitation function.

Another quantity which is useful in the analysis of data is the apparent excitation cross section for the jth level, Q'(j), which is defined as the sum of the direct excitation cross section and the effective cross sections of the cascade from higher levels:

$$Q'(j) = Q(j) + \sum_{i>j} Q(i,j) \quad . \tag{9}$$

The apparent cross section also is given in terms of effective cross sections for states cascading from j to lower levels by the equation,

$$Q'(j) = \sum_{k<j} Q(j,k) \quad . \tag{10}$$

The cascade contribution to the apparent cross section must be subtracted in order to get the true cross section of the jth state.

CHAPTER II

EXPERIMENTAL APPARATUS

Vacuum System

A diagram of the vacuum system used in the experiment is shown in Fig. 1. To achieve and maintain a high vacuum an oil diffusion pump and a molecular-sieve cold trap were used. A major portion of the vacuum system was constructed of stainless steel and mounted on a table whose top was made of insulating material. A specially constructed oven was lowered over this part of the vacuum system to allow continuous bake-out at any desired temperature up to 400 °C. When the system was baked for twelve hours at 200 °C, a pressure below 10^{-7} Torr was attained.

After the initial high vacuum was achieved, the molecular-sieve cold trap was used only to help insure a low impurity gas pressure immediately before an experimental run and to help remove the nitrogen from the system after a run. The oil diffusion pump was allowed to pump continuously on the system between runs. A cold water baffle and a Granville-Phillips Cryosorb cold trap prevented streaming of the oil into the main system. During an experimental run, the background pressure never exceeded 1×10^{-5} Torr.

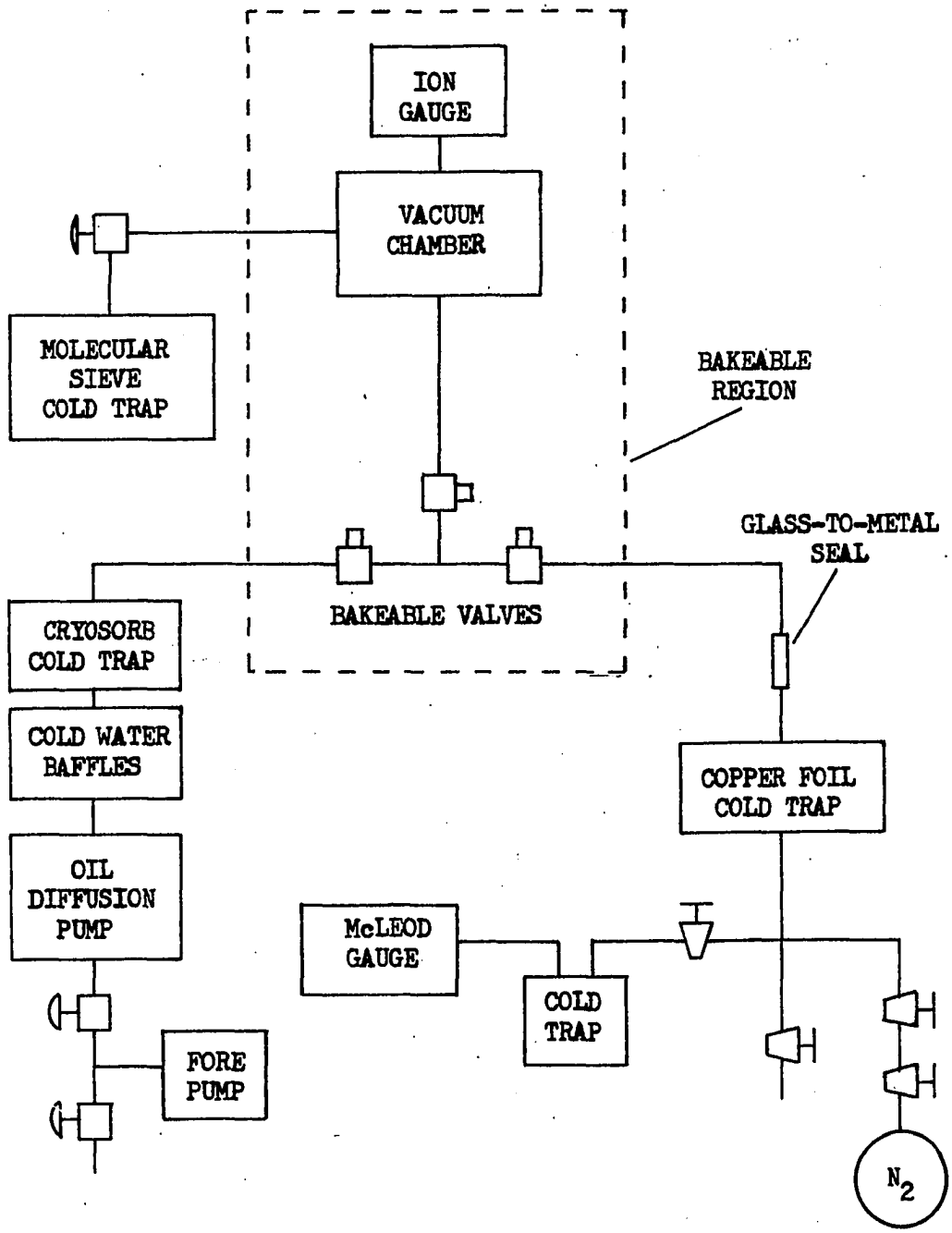

Figure 1. The Vacuum System.

An electron gun was placed in the main vacuum chamber, a stainless steel cylinder 2¼ inches in diameter and 5 inches long. The gun was mounted rigidly on a flange so that it could easily be removed. Two viewing ports, one of pyrex and one of sapphire, were on opposite sides of the chamber. The main vacuum system was connected to the nitrogen source and to a McLeod gauge through a glass-to-metal seal as shown in Fig. 1. The nitrogen was purchased from Linde Company in liter glass bottles, which were permanently attached to the glass portion of the system. The McLeod gauge was used for absolute pressure measurements. A Pirani gauge monitored the pressure after nitrogen was introduced into the system, and an ionization gauge mounted near the main vacuum chamber determined the background pressure.

Optical and Electronic System

Figure 2 shows a block diagram of the arrangement of the electronic and optical components of the experiment. Radiation from the collision chamber of the electron gun was observed in a direction perpendicular to the electron beam. A quartz lens focused an image of the beam on the entrance slit of a monochromator. A ½-meter Jarrell-Ash scanning monochromator with a grating of 1180 lines per mm blazed at 5000 Å was used for the region of the spectrum below 8000 Å: and a ¼-meter Jarrell-Ash monochromator with gratings of 590 and 295 lines per mm blazed at 1.2 and 2.1 microns was utilized for longer wavelengths. Filters removed the second order spectrum from the first order spectrum at long wavelengths.

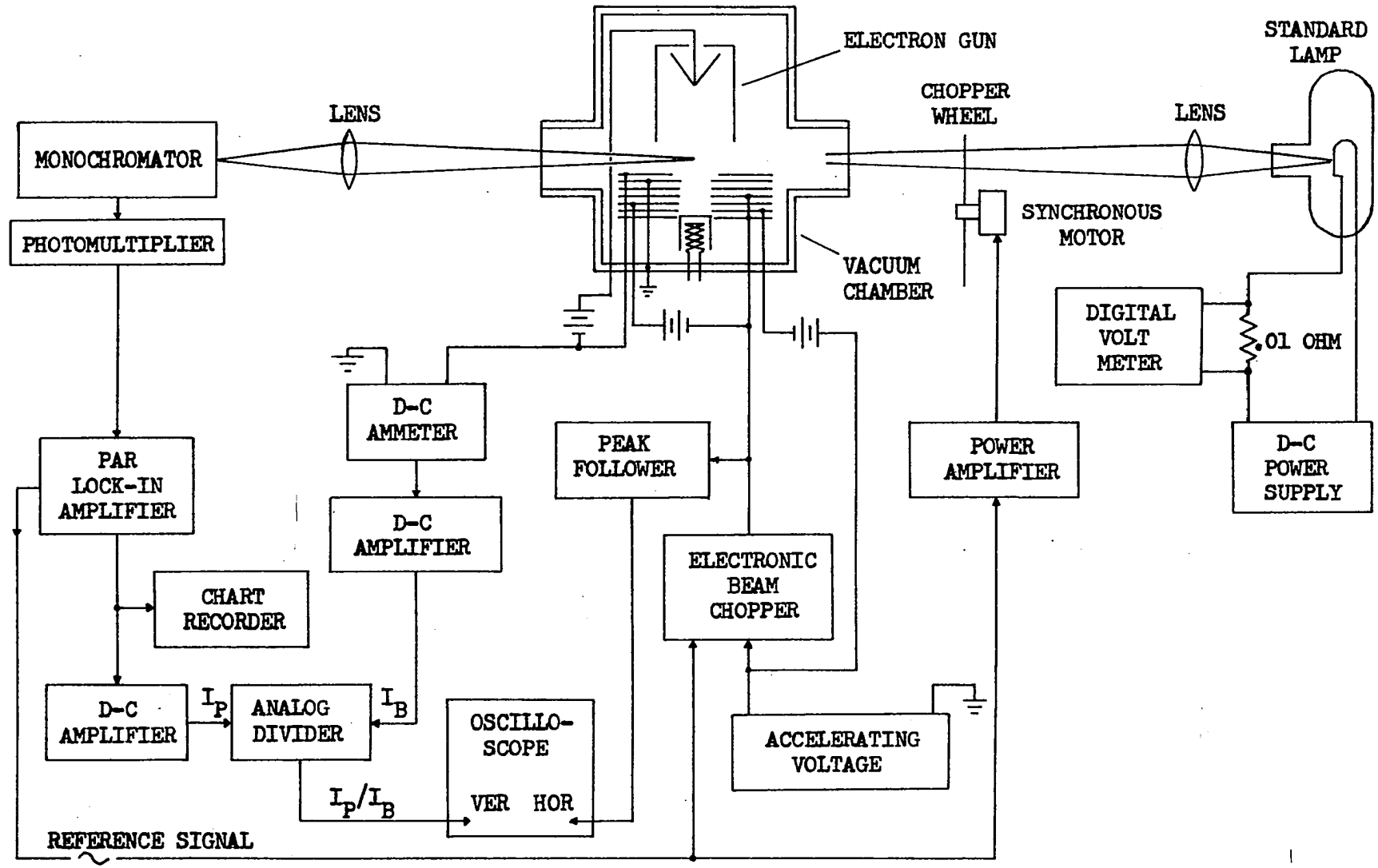

Figure 2. Arrangement of Optical and Electronic Apparatus.

A photomultiplier tube mounted at the exit slit detected the radiation emerging from the monochromator. Four photomultipliers, the EMI 6256B, the EMI 9558, the RCA 7265, and the RCA 7102, were used to cover the spectral range from about 3,000 to 11,000 Angstroms. The RCA 7102 was cooled to liquid nitrogen temperature to reduce its dark current.

The light from the collision chamber was modulated by chopping the accelerating voltage of the electron beam at 90 Hz. The signal from the photomultiplier was reduced in noise and amplified by a Model JB-4 Princeton Applied Research lock-in amplifier. The lock-in amplifier was operated in the internal reference mode and its reference channel sine wave output was used to trigger the electronic beam chopper. The output of the lock-in amplifier (I_p in Fig. 2) was either recorded by a chart recorder or applied to the numerator input of an analog divider.

The electron beam current (I_B in Fig. 2) was measured by an electronic d-c ammeter. The ammeter produced a voltage output which was amplified and applied to the denominator input of the analog divider. The divider produced a signal which was proportional to I_p/I_B. At constant pressure in the collision chamber, I_p/I_B was proportional to the effective cross section. The output of the divider was applied to the vertical deflection plates of an oscilloscope, and the accelerating voltage was applied to the horizontal deflection plates. As the accelerating voltage was slowly varied, the dot on the oscilloscope screen traced out the excitation function. An oscillogram served as a permanent record of the function.

Electron Gun

A more detailed diagram of the electron gun is shown in Fig. 3 The figure is slightly larger than actual size and is drawn to scale. The gun was constructed of stainless steel with glass insulators and nickel grid wires. The inside of the collision chamber was coated with 'Aquadag' to reduce reflections. An externally heated barium impregnated dispenser cathode one cm in diameter was used for the electron source.

The grids of the gun were made of circular stainless steel plates 1/32 inch thick. Electrons from the cathode passed through holes drilled in the centers of these plates. The first four plates had nickel grid wires over the center hole. The grid wires were spot-welded to the plates in a basket weave pattern with a 2 mm spacing between adjacent parallel wires, and the wires on the separate grids were placed so that they lined up with one another.

Holes around the outside edge of the plates were provided for electrical feedthroughs and for support rods. Glass beads placed in undersized holes were used for insulating spacers between the plates. The complete gun assembly was mounted on three stainless steel rods, which were fastened rigidly to a vacuum flange. When the gun was inserted in the vacuum chamber, the outer edges of the plates were about three mm from the chamber walls.

The first grid of the gun was used as a current control and was operated at both positive and negative potentials with respect to

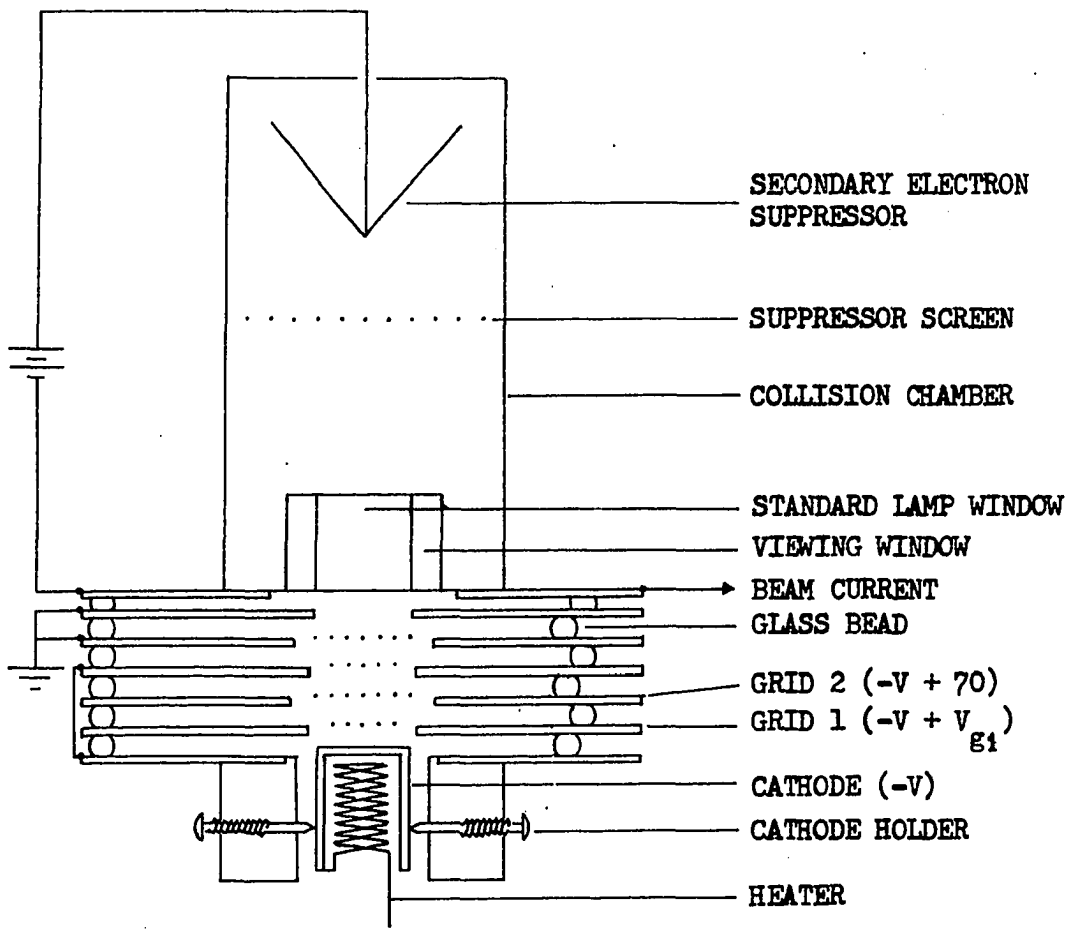

Figure 3. Electron Gun.

the cathode. The second grid, which was operated at about +70 volts with respect to the cathode, accelerated the electrons from the cathode toward the collision chamber. Also, when gas was introduced into the system, the 70 volt electrons passing through the grid created positive ions. At low accelerating voltages these ions drifted into the collision chamber where they helped counteract the space charge of the electron beam. The third grid was connected to the cathode and served as a virtual cathode. The fourth grid was grounded. The accelerating voltage was developed between the fourth grid and the third grid by applying a negative voltage to the cathode. The fifth grid was also grounded. It helped collimate the beam and reduced field penetration into the collision region.

The collision chamber consisted of a cylindrical cup with viewing windows in front and back. A secondary electron suppressor in the end of the cup was held at +9 volts with respect to the cup. The suppressor was cone shaped to reduce the number of electrons reflected back into the collision region. The electric field of the suppressor was screened from the collision region by a nickel wire grid. The electrons of the beam were collected by the collision chamber and the beam current was measured by a d-c ammeter connected between the collision chamber and ground. The voltage drop across the ammeter was negligible so that the collision chamber was approximately at ground potential. In order to modulate the electron beam, the accelerating voltage to the cathode was applied in a square wave which went from the negative accelerating voltage to a positive cut-off voltage. The square wave was supplied by the electronic beam chopper shown in Fig. 4.

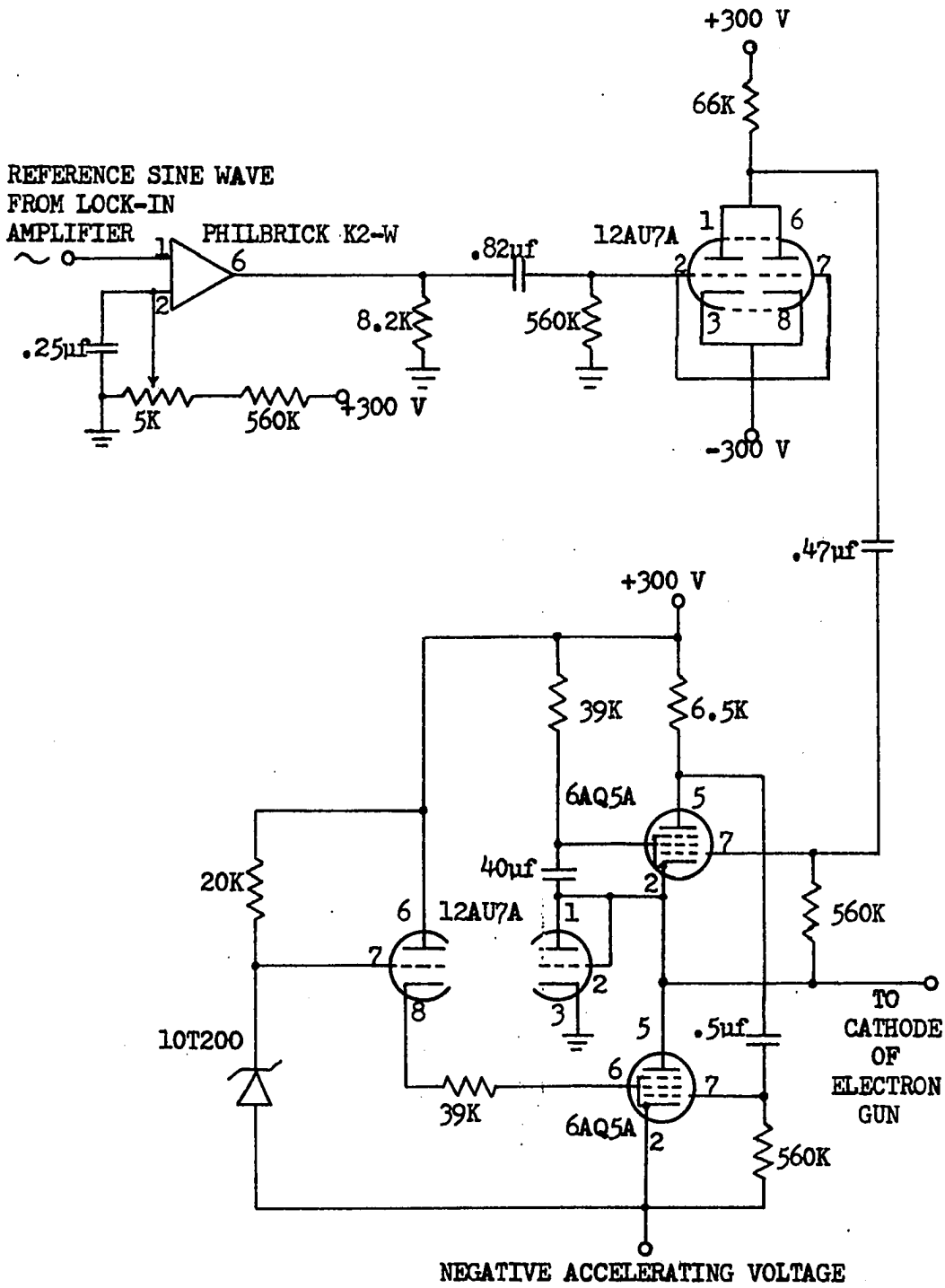

Figure 4. Schematic Diagram of Electronic Beam Chopper.

An estimate of the energy spread of the electron beam was made by applying a positive retarding potential, V_R, to the collision chamber. Only electrons with an energy greater than the retarding potential were collected by the collision chamber and measured as beam current. Figure 5 shows how the beam current varied as V_R was increased when the accelerating voltage was 13 volts and the nitrogen pressure was 5 microns. Figure 5 also shows

$$- \frac{1}{(I_B)_o} \frac{dI_B}{dV_R} ,$$

the negative differential of the I_B versus V_R curve divided by $(I_B)_o$, the beam current at $V_R = 0$. This curve gave the energy distribution of the electrons in the beam. Eighty per cent of the electrons had energies which lay within a spread of 0.6 eV.

A Model 30AT24/13 gas-filled G.E. tungsten strip lamp with a quartz window was used for absolute calibration of the radiation detection system. The lamp was calibrated by the manufacturer in terms of brightness temperature versus d-c current. The current to the lamp was supplied by a regulated d-c power supply. The current was measured with an accuracy of 0.05 per cent by passing it through an 0.01 ohm standard resistor and measuring the voltage drop across the resistor with a Keithly Model 662 digital voltmeter. The light from the standard lamp was mechanically chopped at the same frequency as the modulation of the beam. To insure the proper chopping frequency, the chopper wheel was turned by a synchronous motor which was powered by amplifying

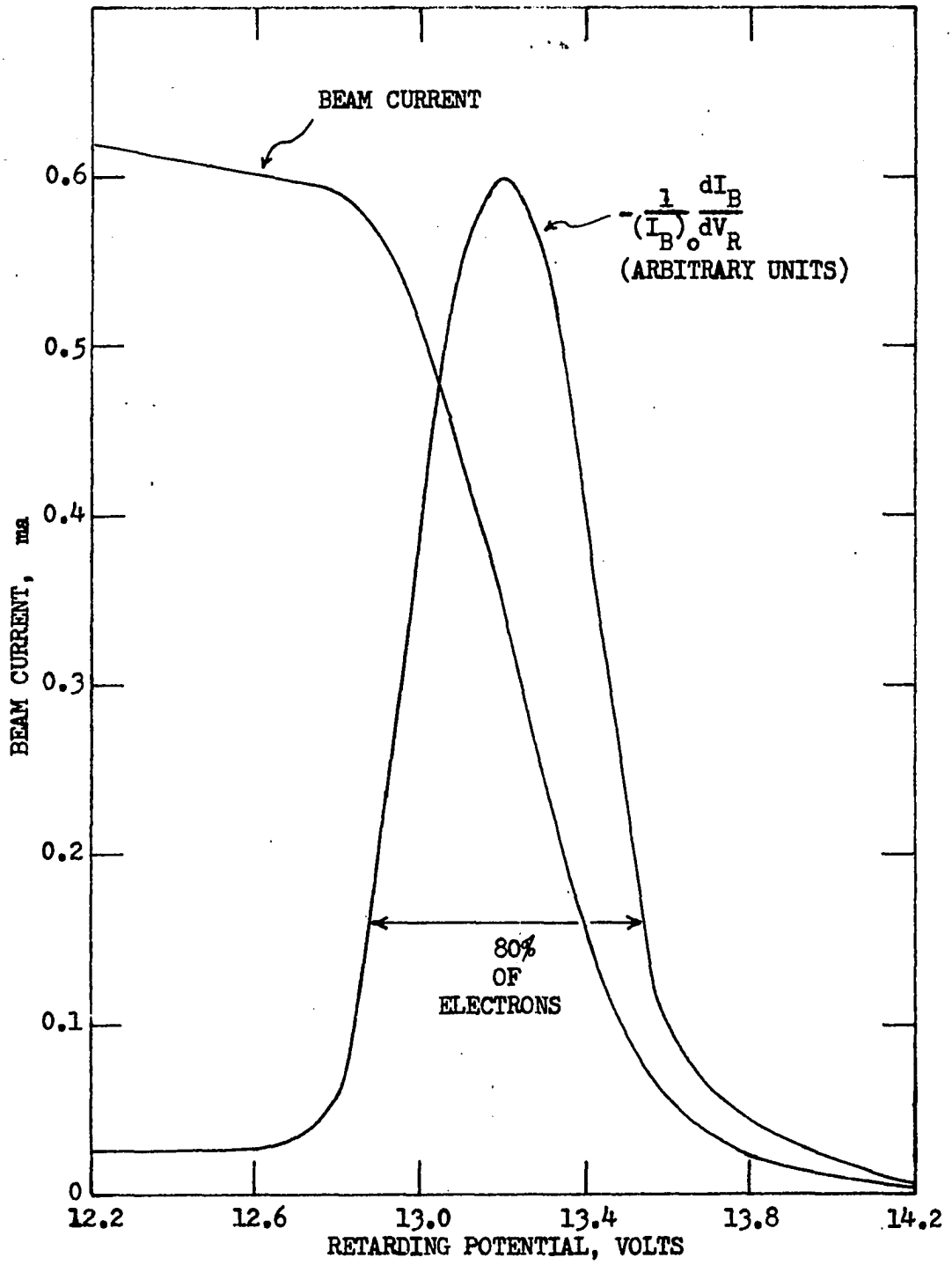

Figure 5. Energy Spread of Electron Beam.

the reference signal from the lock-in amplifier. A more complete discussion of the standardization procedure will be given in the next chapter.

CHAPTER III

MEASUREMENT OF EXPERIMENTAL PARAMETERS

The effective cross section for excitation of the j to k radiative transition was defined in the introduction as

$$Q(j,k) = \frac{e}{I_B N(g)} \int A(j,k)N(j)ds \quad . \tag{11}$$

Let the number of photons emitted per second per unit path length of the electron beam in the j to k transition be defined as R(j,k); then

$$R(j,k) = \int A(j,k)N(j)ds \quad . \tag{12}$$

R(j,k) is proportional to the photomultiplier signal, I_p. The measurement of I_p and the beam current, I_B, were described in the preceding chapter. In this chapter the determination of the ground state density, N(g), and the calibration of the radiation detection system for the absolute determination of R(j,k) will be discussed.

Ground State Density

Under conditions of thermal equilibrium at room temperature, all but a negligible fraction of the N_2 molecules are in the lowest

vibrational level of the ground state. Even at 1000 °K the fraction of molecules not in the lowest vibrational level is small.[15] Therefore, the ground state density may be set equal to the total density, which is related to the pressure by the ideal gas law. Hence

$$N(g) = \frac{P}{kT} \quad , \tag{13}$$

where P is the pressure, k is Boltzmann's constant, and T is the absolute temperature.

The gas in the McLeod gauge, where the pressure was measured, was at room temperature. The hot cathode in the electron gun, however, raised the temperature of the grids and collision chamber walls. When the electron gun was at operating temperature, the gas in the collision chamber was hotter than room temperature. In order to relate N(g) in the collision chamber to the pressure read by the McLeod gauge, it was necessary to know the ratio of N(g) at room temperature to N(g) at the unknown higher temperature.

To determine this ratio, the electron gun was turned off, allowed to cool to room temperature, and then turned on again. Since the effective cross section of a band is proportional to $I_p/I_B N(g)$ at room temperature, it is also proportional to $I_p/I_B P$. Since the effective cross section is constant, any change in $I_p/I_B P$ must be due to a change in N(g). Figure 6 shows the variation of $I_p/I_B P$ with time as the gas heated up after turning the electron gun back on. The ratio of $I_p/I_B P$ at time t = 0 to the same quantity when the gun had reached

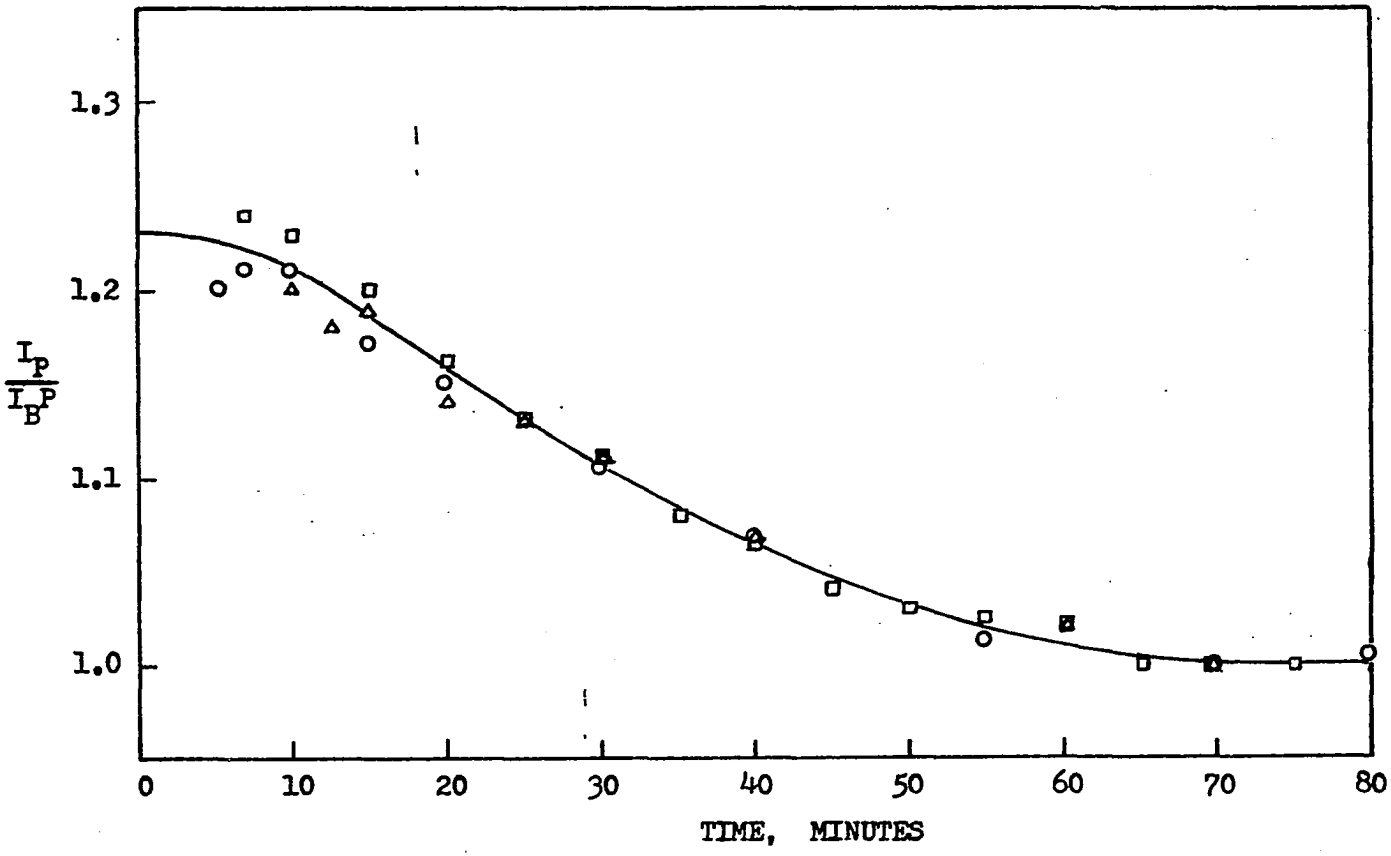

Figure 6. Variation of $I_P/I_B P$ with Time after Turning on Electron Gun.

its normal operating temperature then gave the ratio of N(g) at room temperature to N(g) at operating temperature. This experiment was performed several times at pressures between 4 and 5 microns, and the ratio was found to be 1.23 ±.03.

When a liquid nitrogen cold trap is placed between a McLeod gauge and the chamber whose pressure is being determined, the mercury vapor streaming to the cold trap and condensing causes the pressure in the McLeod gauge to be lower than pressure on the vacuum chamber side of the cold trap.[16] To determine the difference between the two pressures, the neck of the McLeod gauge above the mercury reservoir was cooled with dry ice. The mercury vapor condensed on this neck and did not stream to the cold trap. The intensity of the radiation from the collision chamber with the electron gun's accelerating voltage and beam current held constant was used as a monitor of the pressure in the vacuum chamber. At a pressure between 4 and 5 microns the pressure measured with the neck uncooled was 4 per cent lower than the pressure measured with it cooled.

After corrections were made for the temperature difference between the gas in the collision chamber and the gas in the McLeod gauge and for the pumping action of the McLeod-gauge cold trap, N(g) was found to equal 2.76×10^{13} P molecules/cm^3 at a room temperature of 23 °C when P was measured in microns. Taking into account the 5 per cent accuracy of the McLeod gauge, the maximum possible error in the determination of N(g), after corrections were made, was ± 10 per cent.

Standardization

In order to measure the effective cross section, Q(v',v''), of a molecular band, where v' and v'' are the vibrational quantum numbers of the upper and lower states of the band, it was necessary to determine R(v',v''), the number of photons per second per unit path length emitted by the v' to v'' transition, in terms of known or measurable quantities. Part of this determination involved calibrating the radiation detection system using a standard lamp. The equation expressing R(v',v'') in known or measurable quantities will now be derived.

The radiation of a molecular band is distributed over a range of wavelengths. If the distribution of the radiation in the band is given by G(λ), then

$$R(v',v'') = \int_0^\infty G(\lambda)d\lambda \ , \qquad (14)$$

where λ is the wavelength and the equation refers to an individual band. G(λ) has units of photons/sec/Å/cm. If the radiation is unpolarized, then it is isotropic; and the fraction of R(v',v'') that enters the monochromator is given by $\frac{\Omega}{4\pi}$, where Ω is the solid angle of the radiation originating from the collision chamber and entering the monochromator. It has been assumed that Ω is approximately constant for all portions of the beam observed.

Let T(λ,Λ) be defined as the response of the photomultiplier, monochromator, and lens combination (hereafter referred to as the detection system) to a monochromatic incident flux of one photon/sec and

of wavelength λ when the monochromator wavelength counter is set at Λ. The response of the detection system to $G(\lambda)$ as a function of the monochromator setting Λ is then

$$I_p = \frac{L\Omega}{4\pi} T_o \int_0^\infty G(\lambda)T(\lambda,\Lambda)d\lambda \ , \tag{15}$$

where L is the effective length of the portion of the electron beam observed and T_o is the transmittance of the vacuum chamber viewpoint. If a band is scanned by the monochromator, $I(v',v'')$, the integrated intensity of the band, is defined as the area under the I_p versus Λ curve for the scan of the band. From this definition and Eq. (15),

$$I(v',v'') = \frac{L\Omega}{4\pi} T_o \int_0^\infty\int_0^\infty G(\lambda)T(\lambda,\Lambda)d\lambda d\Lambda \ . \tag{16}$$

Changing the order of integration of the double integral in Eq. (16) gives

$$\int_0^\infty\int_0^\infty G(\lambda)T(\lambda,\Lambda)d\lambda d\Lambda = \int_0^\infty [\int_0^\infty T(\lambda,\Lambda)d\Lambda]G(\lambda)d\lambda \ . \tag{17}$$

$\int_0^\infty T(\lambda,\Lambda)d\Lambda$ is the area under the scan of a monochromatic incident flux of one photon/sec, and is a slowly varying function of λ when compared with $G(\lambda)$. Since the radiation from a band extends over a limited range of wavelengths, $G(\lambda)$ for the band is equal to zero outside this range. Therefore, the right-hand side of Eq. (17) may be expressed approximately as

$$[\int_0^\infty T(\lambda_o,\Lambda)d\Lambda] \int_0^\infty G(\lambda)d\lambda$$

where λ_o corresponds to the wavelength of a spectral feature of the band. The accuracy of the approximation depends on the choice of λ_o. Substituting $\int_o^\infty T(\lambda_o,\Lambda)d\Lambda \int_o^\infty G(\lambda)d\lambda$ in Eq. (16) and solving for $\int_o^\infty G(\lambda)d\lambda$ gives

$$R(v',v'') = \int_o^\infty G(\lambda)d\lambda = \frac{4\pi I(v',v'')}{L\Omega T_o \int_o^\infty T(\lambda_o,\Lambda)d\Lambda} . \tag{18}$$

The quantity, $\int_o^\infty T(\lambda_o,\Lambda)d\Lambda$, in Eq. (18) can be expressed in terms of the response of the detection system to radiation from the standard lamp. With the monochromator wavelength counter set at Λ, the response of the detection system to the standard lamp is

$$I_s(\Lambda) = \int_o^\infty B(\lambda)T(\lambda,\Lambda)d\lambda , \tag{19}$$

where $B(\lambda)$ is the spectral irradiance due to the standard lamp and is assumed to be known. Since $B(\lambda)$ is a slowly varying function of λ, $I_s(\Lambda)$ in Eq. (19) may be written approximately as

$$I_s(\Lambda) = B(\Lambda) \int_o^\infty T(\lambda,\Lambda)d\lambda , \tag{20}$$

where $B(\lambda)$ has been taken from under the integral sign and given the value $B(\Lambda)$.

Dividing both sides of Eq. (20) by $B(\Lambda)$ gives

$$I_s(\Lambda)/B(\Lambda) = \int_o^\infty T(\lambda,\Lambda)d\lambda . \tag{21}$$

Let λ_o equal Λ_o; then

$$\int_0^\infty T(\lambda_o,\Lambda)d\Lambda = \int_0^\infty T(\lambda,\Lambda_o)d\lambda \ . \tag{22}$$

From Eqs. (21) and (22)

$$\int_0^\infty T(\lambda_o,\Lambda)d\Lambda = I_s(\Lambda_o)/B(\Lambda_o) \ . \tag{23}$$

Using Eq. (23), Eq. (18) may now be written in terms of known or measurable quantities as

$$R(v',v'') = \frac{4\pi I(v',v'')B(\Lambda_o)}{L\Omega T_o I_s(\Lambda_o)} \ . \tag{24}$$

For a discussion of the errors involved in the approximations leading to Eq. (24) see the article by Merrill and Layton entitled "The Calibration of Scanning Monochromators for the Measurement of Absolute Irradiance".[17] (Much of the notation used in the preceding discussion has been adapted from the Merrill and Layton article.)

The spectral irradiance due to the standard lamp, which was assumed to be known when it was introduced in Eq. (19), can be written as

$$B(\lambda) = T_s A_s \Omega_s P(\lambda,T) \ , \tag{25}$$

where T_s is the transmission of all optical components between the standard lamp ribbon and the detection system, A_s is the effective area of the standard lamp ribbon, and Ω_s is the solid angle of the

radiation originating from the ribbon. $P(\lambda,T)$ is the number of photons per second per unit solid angle per unit wavelength emitted by a tungsten ribbon at a true temperature T and wavelength λ in a direction perpendicular to the surface of the ribbon. The true temperature of the standard lamp ribbon was derived from its brightness temperature by using DeVos' data on the emissivities of tungsten,[18] and Wien's black body radiation law. $P(\lambda,T)$ was obtained from a table which had been generated by a computer program using DeVos' emissivities, and Planck's black body radiation law.[19]

Using the expression for $B(\lambda)$ given in Eq. (25), Eq. (24) may now be written as

$$R(v',v'') = 4\pi \frac{A_s \Omega_s}{L\Omega} \frac{T_s}{T_o} \frac{P(\lambda,T)}{I_s(\lambda_o)} I(v',v'') \quad . \tag{26}$$

The absolute calibration of the radiation detection system was carried out with the standard lamp in two different positions. Figure 7a shows the first position, the standard lamp placed behind the collision chamber. A quartz lens focused an image of the standard lamp tungsten ribbon at a plane in the center of the collision chamber by passing light from the standard lamp through a viewing window in the vacuum chamber and through a hole in the back of the collision chamber. A second image of the ribbon was then formed on the monochromator entrance slit by the lens between the collision chamber and monochromator.

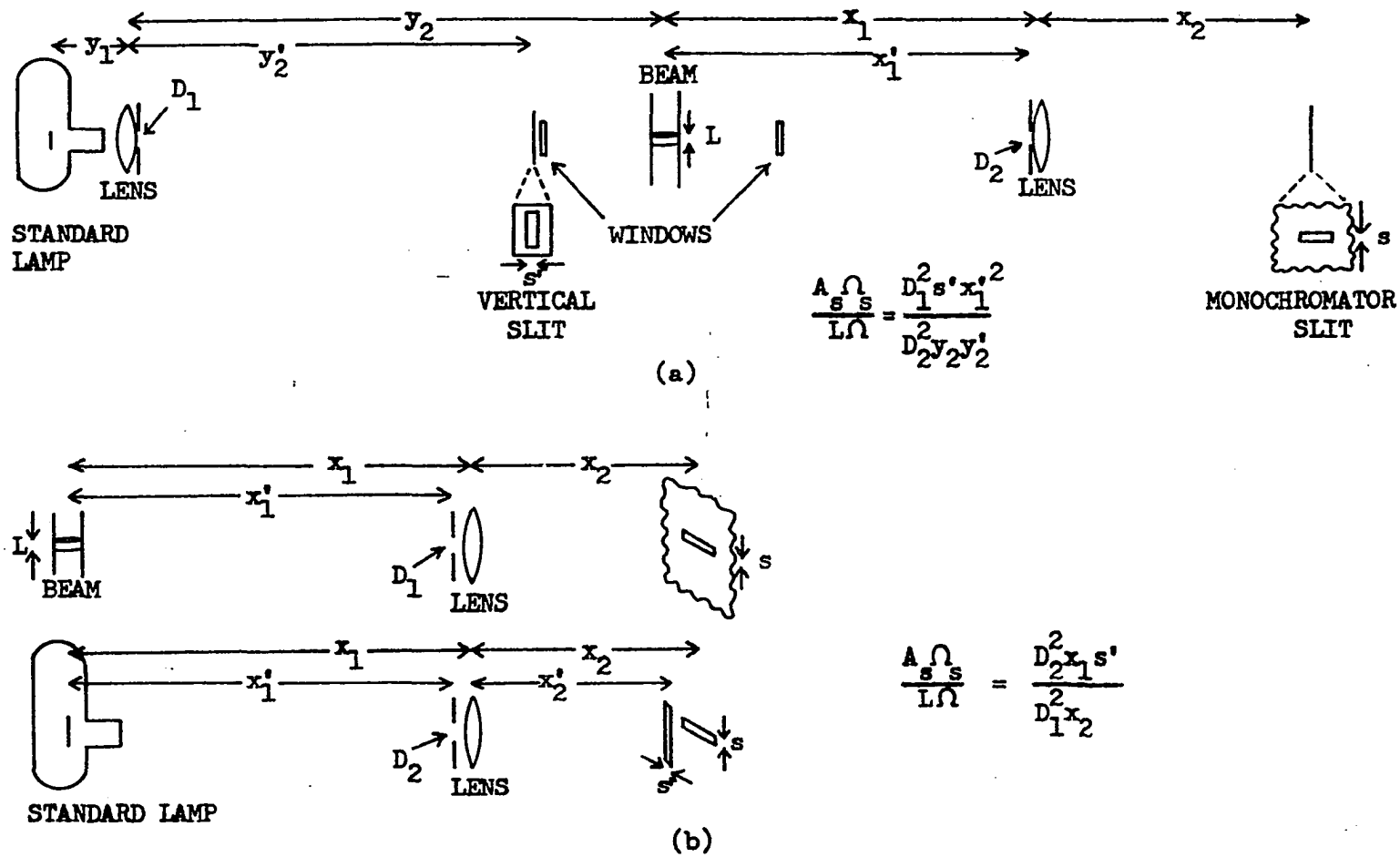

Figure 7. Two Arrangements for Standardization.

With the standard lamp in the first position, the solid angle Ω_s was determined by placing an aperture stop at the first lens. The effective area A_s was determined in the vertical direction by the monochromator slit and in the horizontal direction by a slit placed in front of the back window of the collision chamber. The transmittance, T_s, was obtained by multiplying the transmittances of the standard lamp window, the standard lamp lens, and the vacuum chamber windows. The transmittances were taken from a note published by Varian which gave the transmittance versus wavelength curves for vacuum windows made of various materials.[20] The detection system could be calibrated without moving any of the optical components with the lamp in the first position.

The standard lamp was also mounted in a position adjacent to the vacuum chamber as shown in Fig. 7b. The monochromator was turned so that the standard lamp ribbon occupied the same position relative to the monochromator as was formerly occupied by the center of the collision chamber. An aperture stop placed in front of the monochromator lens determined the standard lamp solid angle. The horizontal monochromator entrance slit and a vertical slit placed in front of the monochromator slit determined the effective area of the standard lamp ribbon. With this arrangement, the optical paths of the light from the collision chamber and from the standard lamp differed less than with the first arrangement.

The radiation from the collision chamber had a linear magnification of ½ so that the image of the one cm beam on the monochromator slit irradiated only the center portion of the slit. The width of the slit determined the effective length, L, of the part of the beam observed. For strong bands, the solid angle Ω of the light from the collision chamber was determined by placing an aperature stop in front of the monochromator lens. For weak bands, the aperture stop was removed, and the light allowed to flood the monochromator. The monochromator grating and light baffles then defined Ω, which was measured by multiplying the ratio of I_p with the stop out to I_p with the stop in times the solid angle with the stop in place. The value of the solid angle with the stop removed depended on the monochromator wavelength setting since the f-number of the monochromator changed with the inclination of the grating.

When using the aperture stop to determine Ω or Ω_s, care must be taken that none of the light entering the monochromator strikes a baffle or falls off the grating. A visual check was made by looking through the exit slit to observe if light from a strong line or from the standard lamp overlapped the edge of the grating. In order to see the edges of the grating, the monochromator cover was removed, and the room lights were allowed to illuminate the grating.

There were several sources for error in the calibration of the detection system. The response of a photomultiplier was not uniform over the face of its cathode, and the intensity of the radiation from the collision chamber and from the standard lamp were not distributed

identically over the face of the photomultiplier cathode. A check was made to see if this nonuniformity caused an error in the calibration. No appreciable change in the value obtained for a cross section of a band was observed when the photomultiplier was rotated or when two different photomultipliers were used. It was assumed, therefore, that no appreciable errors in the calibration were introduced by the non-uniformity of the photo-cathode.

In the case of the first standard lamp arrangement, the non-uniformity of the grating was checked for its influence on the calibration. The light from the standard lamp occupied a much smaller area of the grating than the light from the collision chamber. When the light from the collision chamber was stopped down until it illuminated the same portion of the grating as the light from the standard lamp, I_p was found to vary linearly with the area of the stop. Thus, it appeared that little error was introduced by nonuniformity of the grating.

The two optical arrangements for standarization are shown in Fig. 7 and the relation of $A_s\Omega_s/L\Omega$ to the geometrical measurements is given for both cases. $A_s\Omega_s/L\Omega$ was determined with an accuracy of better than 1 per cent. The error introduced by nonuniformities in the grating and the photo-cathodes were judged to be less than 3 per cent. The error due to an incorrect choice of λ_o for a band was less than 3 per cent at long wavelengths where the detection system response was changing rapidly with λ and the bands were over 100 angstroms wide; the error was less than 1 per cent elsewhere. The accuracy of the manufacturer's calibration of the standard lamp and the deviation of the tungsten ribbon

emissivities from the emissivities measured for tungsten by DeVos were unknown.

The standard lamp was operated at a true temperature of 2000 °K for standardization at short wavelengths and at 1800 °K for long wavelengths. The error in the intensity per unit wavelength emitted by a black body at 2000 °K at 3000 angstroms is 1.2 per cent per °K of error in temperature. The error at 1800 °K and 11,000 angstroms is 0.4 per cent per °K. Errors at wavelengths between 3000 angstroms and 11,000 angstroms lie between 0.4 per cent and 1.2 per cent per °K temperature error.

CHAPTER IV

FIRST POSITIVE SYSTEM

The first positive band system of nitrogen appears readily in the positive column of a d-c discharge in nitrogen or air and is a prominent feature of the spectrum of the aurora. The system extends from the infrared down through the visible region of the spectrum. In this work bands between 5300 angstroms and 10,500 angstroms were studied. The upper levels of the first positive system are the vibrational levels of the $B^3\pi_g$ electronic state, and the lower levels are the vibrational levels of the $A^3\Sigma_u^+$ electronic state. The $B^3\pi_g$ - $A^3\Sigma_u^+$ transition is the only transition from the $B^3\pi_g$ state which is allowed by the selection rules for electric dipole radiation.

The partial energy level diagram of N_2 in Fig. 8 shows the $A^3\Sigma_u^+$ and $B^3\pi_g$ electronic states with respect to the ground $X^1\Sigma_g^+$ state. The diagram also shows the states which cascade into the $B^3\pi_g$ state. The heavier lines on the diagram indicate the v = 0 vibrational levels of the electronic states and the shorter, thinner lines mark the higher vibrational levels of the states. Four states which cascade into the $B^3\pi_g$ state have been identified. They are $B'^3\Sigma_u^-$ (infrared afterglow system), $C^3\pi_u$ (second positive system), $C'^3\pi_u$ (Goldstein-Kaplan bands), and $D^3\Sigma_u^+$ (fourth positive system).[21]

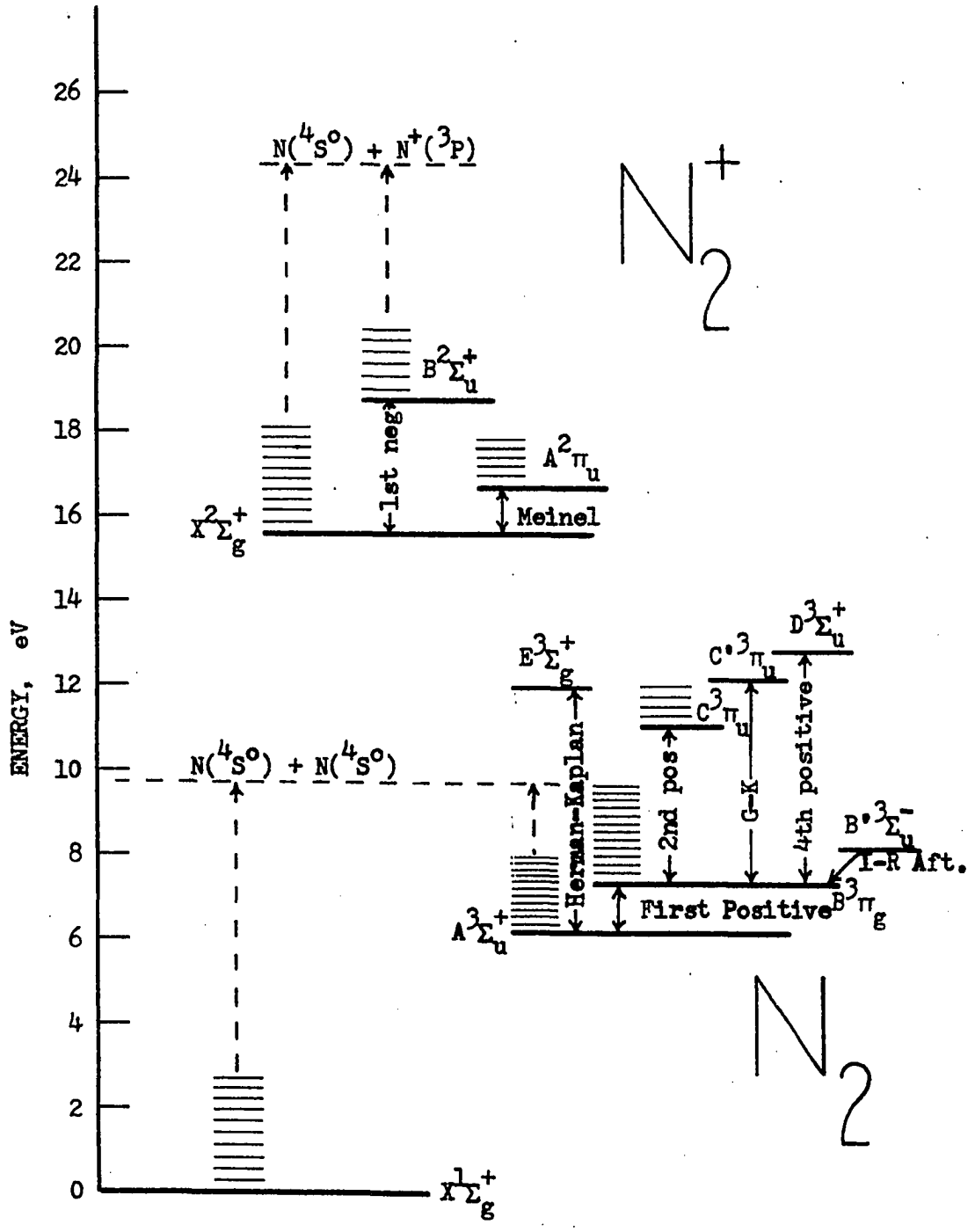

Figure 8. Partial Energy Level Diagram of Molecular Nitrogen.

In the derivation of the cross section expression in Chapter I, it was assumed that direct electron excitation of the ground state molecules and cascade were the only significant excitation and de-excitation processes. Of the previously neglected processes all but one are non-linear with pressure or beam current, and can be made negligible by operating at low pressures and beam currents. A plot of I_p versus P for the (6,3) first positive band at an electron energy of 12 eV (I_B constant) was linear for P less than 15 microns, but at 30 eV was not linear until P was less than 3 microns. I_p versus I_B (P constant and less than 6μ) was linear for beam currents up to 2 ma, the maximum current used in the experiment. All absolute measurements in the first positive system were made at electron energies between 10 and 12 eV and at pressures below 6 microns, and any measurements at higher energies were made at pressures below 3 microns. Therefore, the processes non-linear with P and I_B could be safely neglected.

The linear process neglected in the derivation of the cross section expression was also found to be small under experimental conditions. Excited molecular states which have long lifetimes can drift from the region of the electron beam under observation or collide with the collision chamber walls before radiating. M. Jeunehomme found the lifetimes of vibrational levels of the $B^3\pi_g$ state extrapolated to zero pressure to lie between 4×10^{-6} sec and 8×10^{-6} sec.[22] A check was made to see if the lifetimes of the $B^3\pi_g$ state were long enough to cause errors in the first positive effective cross section measurements.

With the monochromator turned so that its slits were parallel to the direction of the electron beam, radiation from the collision chamber at different distances from the center of the electron beam was observed. The variation of the light intensity from the (6,3) first positive band with distance x from the center of the beam is shown in Fig. 9. For comparative purposes, a similar curve for the (0,2) band of the second positive system is also shown. Since the second positive system has lifetimes of the order of 5×10^{-8} sec,[23] the radiation from the (0,2) band was emitted only from the region occupied by the electron beam. With the curves for the first and second positive bands normalized to the same value at their peaks, the curve for the first positive band lay above that of the second positive band for all x except at the point of normalization. The position of the curves indicated that part of the radiation from the first positive band was being emitted from outside the electron beam. From these curves it was estimated that less than 10 per cent of the radiation from the (6,3) band was lost from observation by diffusion of excited molecules beyond the edges of the viewing window, and no attempt was made to correct for diffusion losses.

Relative Excitation Functions

The effective excitation function of a band gives the variation of its effective cross section with the incident energy of the electrons. The relative effective excitation functions of the first positive bands which have the same upper vibrational state v', but which possess

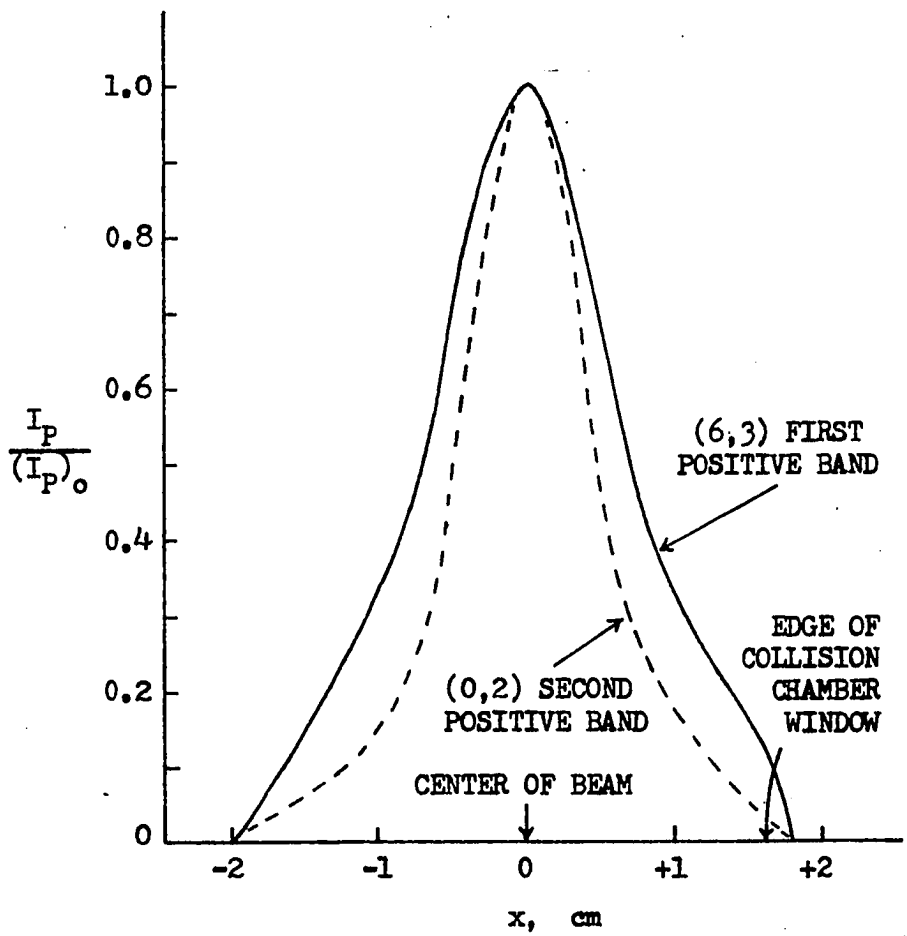

Figure 9. Variation of I_p with Distance of Region of Observation from Center of Electron Beam.

different lower vibrational states v", have the same shape since the effective cross sections for all bands in a v"-progression differ only by the ratio of their Einstein coefficients for emission A(v',v"), and the A(v',v") are independent of electron energy. The relative excitation functions of the first positive bands with 10 different values of v' are shown in Figs. 10 and 11.

To remove the effects of contact potentials and space charge on the relation between the measured accelerating voltage and the energy of the electrons, the energy scales of the excitation functions in Figs. 10 and 11 were adjusted so that onset of excitation of the 3371 Å $N_2(0,0)$ second positive band ($C^3\pi_u$ - $B^3\pi_g$) occurred at 11.0 eV, the spectroscopic value of the energy above ground state of the lowest vibrational level of the $C^3\pi_u$ state.[24] The onset was determined by extrapolating to zero the linear portion of the excitation function of the (0,0) second positive band at threshold. After the energy scales were adjusted by a constant amount, the onsets of excitation of the first positive bands occurred approximately at the spectroscopic value of the $B^3\pi_g$ vibrational energy levels. Thus the onset electron energy of a band depended on the value of v' for the band.

The excitation functions in Figs. 10 and 11 have several features in common. Each curve exhibits a sharp maximum at about 2.6 to 3.0 eV past onset of excitation, and then passes through a second sharp maximum at an electron energy of from 15 to 16 eV. At still greater electron energies, the curves drop rapidly; and at 50 eV the

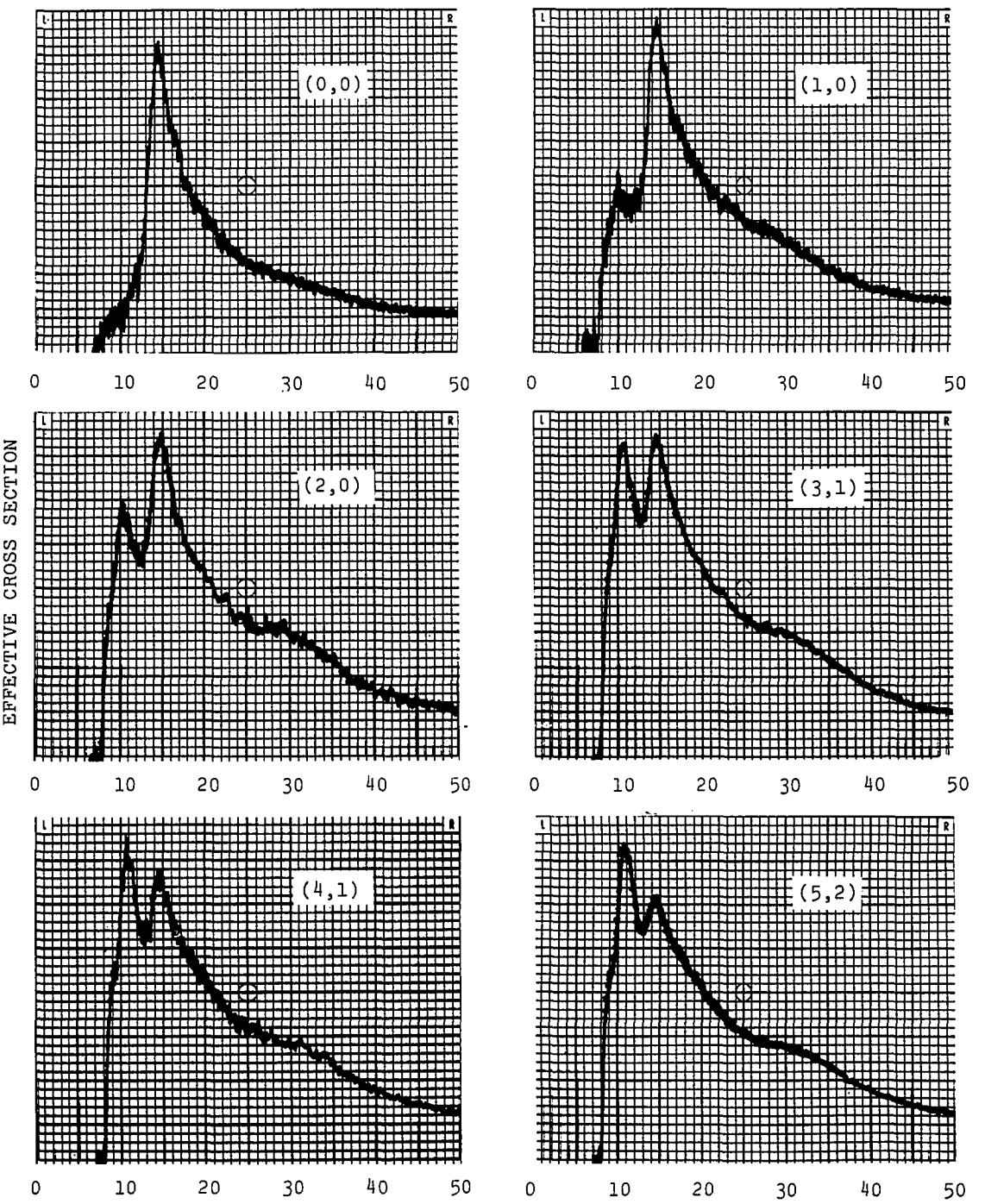

Figure 10. Relative Excitation Functions of N_2 First Positive Bands with v' = 0 through 5.

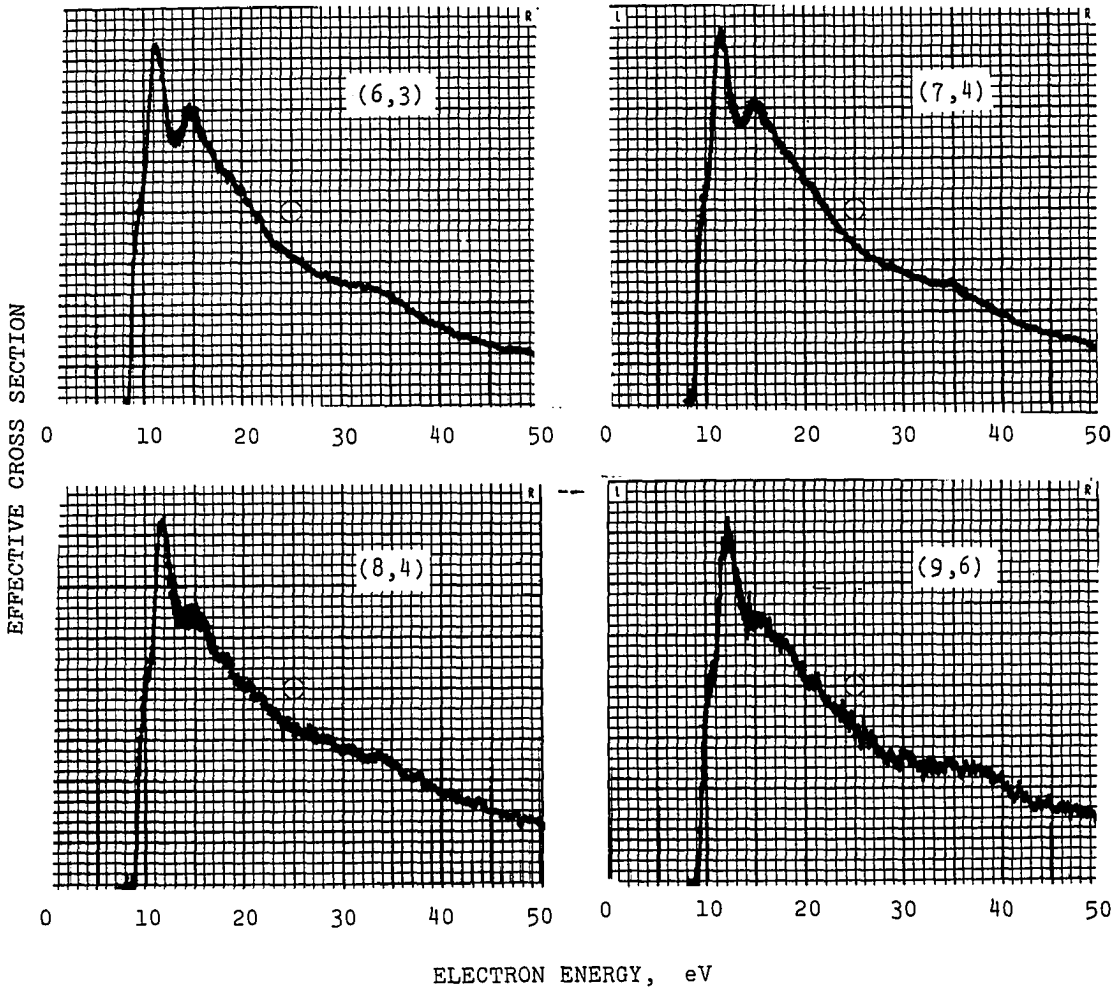

Figure 11. Relative Excitation Functions of N_2 First Positive Bands with v' = 6 through 9.

effective cross sections are less than 20 per cent of their previous high values at lower energies. The second maximum dominates the first in the excitation function for the (0,0) band, but the height of the second maximum of the other curves decreases relative to that of the first maximum as the vibrational quantum number v' increases. The second peak in the first positive excitation function is caused mainly by cascade from the second positive system. Therefore, the excitation functions in Figs. 10 and 11 indicate that the second positive cascade is the major populating mechanism for the lowest vibrational level of the $B^3\pi_g$ state for electron energies above 13 eV and that the second positive cascade decreases in importance as v' increases.

When the electron energy exceeded 16.7 eV, the N_2^+ Meinel band system began to be excited. The Meinel bands overlapped many of the first positive bands with wavelengths above 6100 Angstroms; thus the high electron energy tails of the excitation functions of these overlapped first positive bands were too high. Some first positive bands were also overlapped by atomic lines from dissociated N_2 and by N_2^+ first negative bands. Special care was exercised to exclude unwanted radiation from the determination of the excitation functions in Figs. 10 and 11.

When the thresholds of the first positive excitation functions are plotted on an expanded energy scale, an abrupt change in slope of the curves approximately midway between onset and the first peak is revealed. Figs. 12 and 13 show this change in slope for bands with

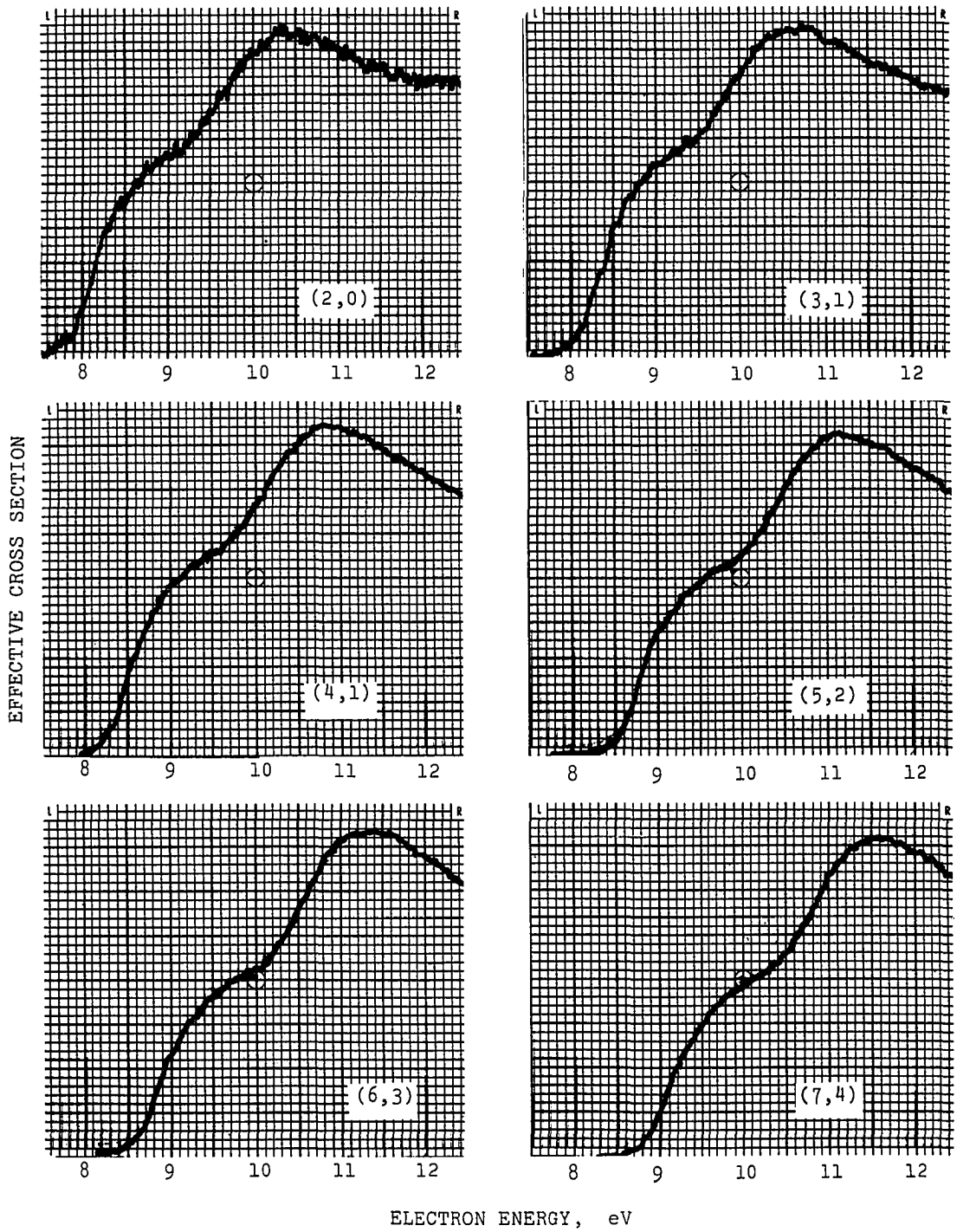

Figure 12. First Positive Excitation Functions at Threshold. v' = 2 through 7.

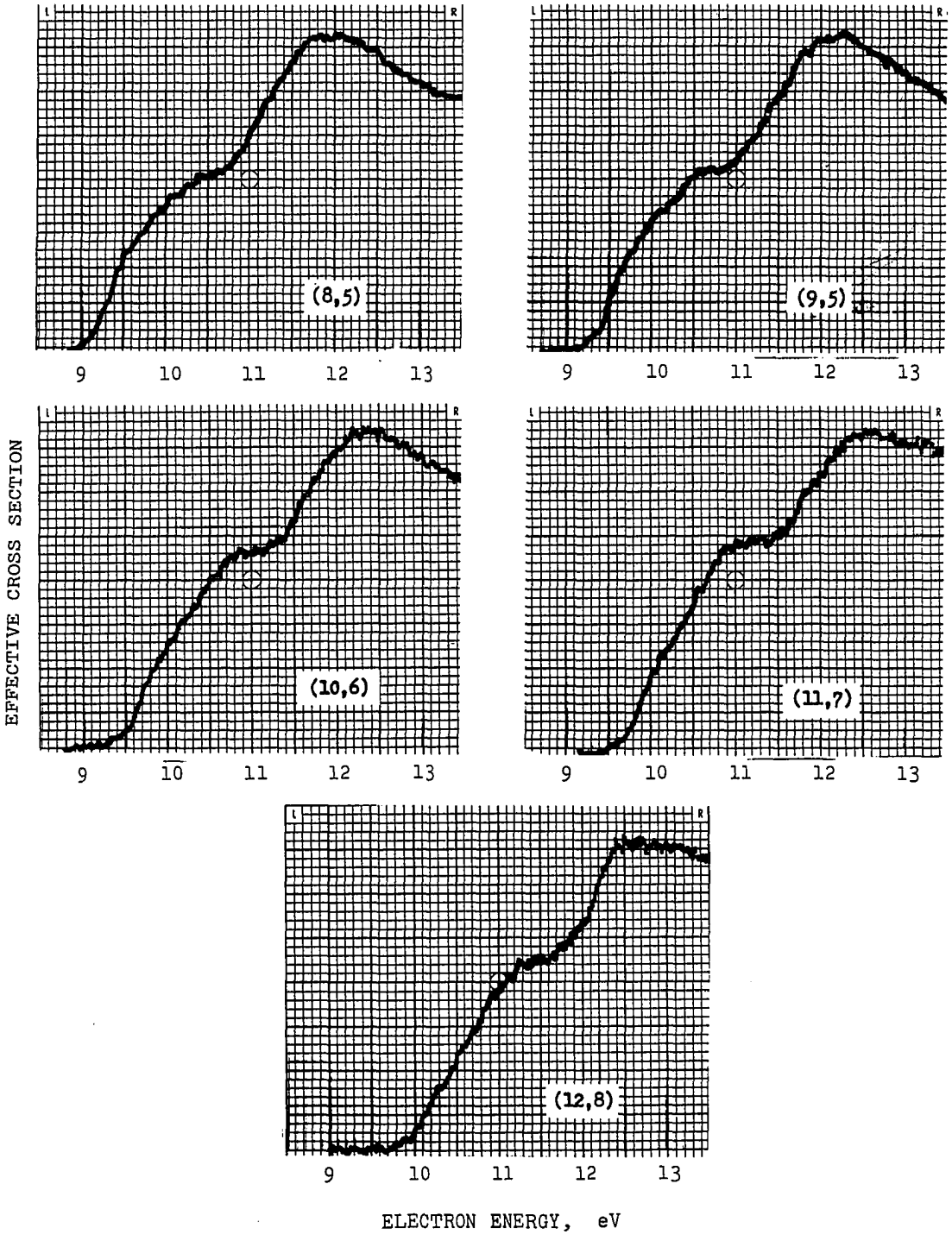

Figure 13. First Positive Excitation Functions at Threshold. v' = 8 through 12.

v' = 2 through v' = 12. The electron energy between onset and the first peak increased linearly with v' from an energy of 2.3 eV for v' = 1 to 3.0 eV for v' = 12.

Absolute Effective Cross Sections

Table 1 summarizes the results of the measurement of the absolute effective cross sections for 39 bands of the N_2 first positive system at the electron energy of the first sharp peak in their excitation functions. The error limits shown for each measurement are an estimate of the uncertainty of the relative measurements within the first positive system. The absolute accuracy of the effective cross sections is estimated to be 20 per cent.

In Chapter III the absolute effective cross section of a molecular band Q(v',v'') was expressed in terms of the integrated intensity of the band, I(v',v''). The integrated intensity was defined as the area under the spectral scan of the band. Quite often two or more bands overlap in a region of the spectrum. A scan of the N_2 spectrum from 5700 angstroms to 6200 angstroms excited by 12 eV electrons is shown in Fig. 14. The use of 0.4 mm slits gave a monochromator band pass half-width of 6 angstroms and resulted in a blending of the rotational structure of the bands. The scan shows that there was serious overlapping of the first positive bands in the $\Delta v = 4$ sequence (bands for which v' - v'' = 4). For shorter wavelength bands with $\Delta v > 4$, the overlapping was greater than for $\Delta v = 4$, while for longer wavelength bands with $\Delta v < 4$, the overlapping diminished until adjacent bands in a

Table 1. Effective Electron Excitation Cross Sections of First Positive Bands of N_2 at the Electron Energy of the Maximum of the First Sharp Peak in Their Excitation Functions (10^{-18} cm^2).

v'-- v''	0	1	2	3	4	5	6	7	8	9	10	11	12
0	2.2 ±.3	5.4 ±.6	4.1 ±.1	0.97 ±.02		0.009 .001							
1			5.3 ±.5	6.2 ±.2	2.18 ±.04	0.29 ±.01	0.018 ±.001						
2			1.1 ±.1	1.7 ±.2	5.45 ±.10	2.60 ±.05	0.48 ±.02	0.029 ±.002					
3				2.2 ±.2		3.04 ±.06	2.52 ±.05	0.51 ±.02	0.038 ±.002				
4					1.9 ±.2		1.45 ±.05	1.65 ±.05	0.40 ±.02	0.042 ±.002			
5						1.1 ±.2		0.44 ±.02	0.94 ±.03	0.31 ±.01	0.033 ±.002		
6										0.47 ±.01	0.218 ±.009	0.36 ±.02	
7											0.246 ±.010	0.170 ±.007	0.038 ±.002
8												0.121 ±.005	0.140 ±.006

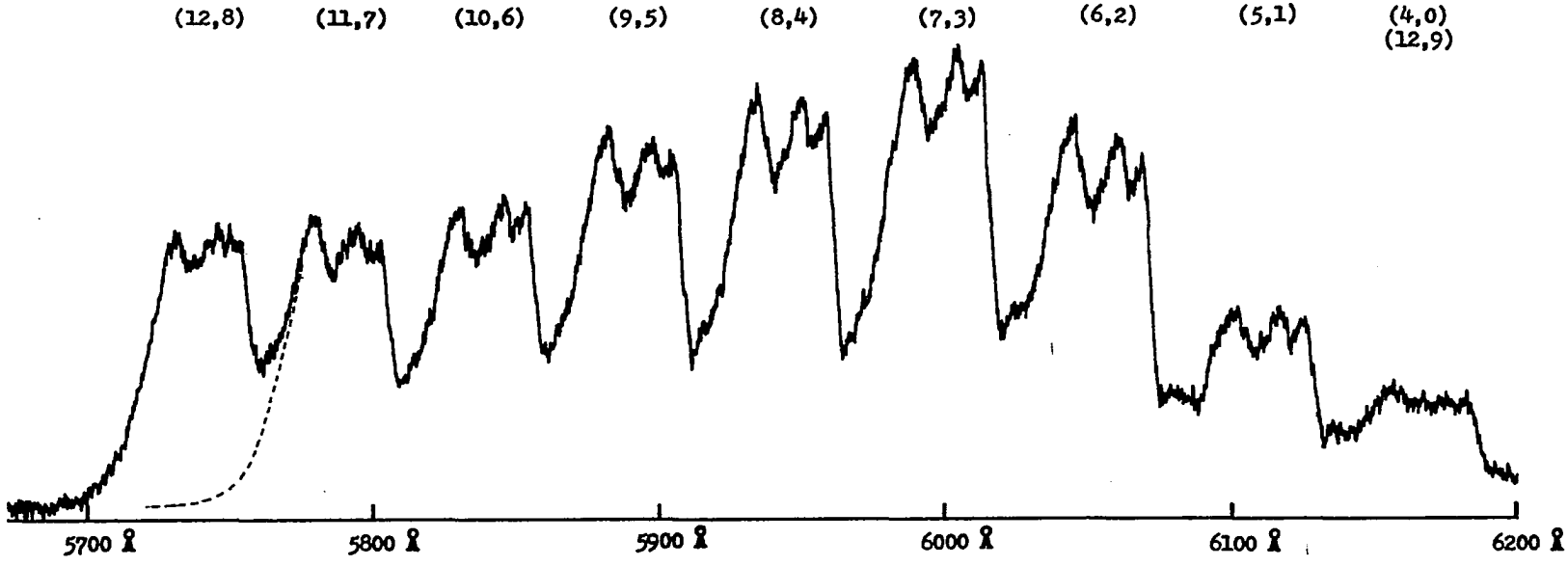

Figure 14. Scan of N_2 Spectrum from 5700 Å to 6200 Å Excited by 12 eV Electrons.

sequence were well separated. In addition to overlapping of adjacent bands in a sequence there was some overlapping of sequences. The (4,0) band in the $\Delta v = 4$ sequence was overlapped exactly by the (12,9) band in the $\Delta v = 3$ sequence; the (3,0), (4,1), and (5,2) bands in the $\Delta v = 3$ sequence were overlapped by the (10,8), (11,9), and (12,10) bands in the $\Delta v = 2$ sequence, and so on. When two or more adjacent bands in a sequence overlapped in a region of the spectrum or when bands from different sequences overlapped, a method of separating the radiation which came from each band had to be devised.

To correct for the overlapping of adjacent bands in a sequence, the tail of each band was extended and the amount that the tail contributed to the integrated intensity of the band it overlapped was subtracted. Under low resolution the first positive bands appeared to have three band heads degraded to shorter wavelengths. The short wavelength tail of the (12,8) band (Fig. 14) was not overlapped. Therefore, the shape of the overlapped tails of the other bands in the $\Delta v = 4$ sequence were deduced from the shape of the (12,8) band. By extending the tail of the (11,7) band, as shown by the dotted line in Fig. 14, it was possible to subtract its contribution to the integrated intensity of the (12,8) band. The overlap of the other bands were separated in a similar manner. The errors involved in this method of separating the overlaps were greatest for the $\Delta v = 5$ sequence and for weak bands which were overlapped by the tails of strong bands.

To determine $Q(v',v'')$ for a band which was overlapped by a band in another sequence, the sum of the effective cross sections of the

bands was measured using the total integrated intensity of the two overlapping bands. Franck-Condon factors calculated by Zare, Larsson, and Berg[25] for the first positive system were used to calculate theoretical relative transition probabilities for emission,

$$A_R(v',v'') = \frac{A(v',v'')}{\sum_{v''} A(v',v'')} . \tag{27}$$

The relative transition probabilities were utilized to determine the apparent cross sections $Q'(v)$ for each vibrational level of the $B^3\pi_g$ state from the measured effective cross sections. The equation,

$$Q(v',v'') = A_R(v',v'')Q'(v') \tag{28}$$

then gave an estimate of $Q(v',v'')$ for the weaker of the two overlapping bands. To get the effective cross section of the stronger band, the $Q(v',v'')$ for the weaker band was subtracted from the total effective cross section of the overlapping bands. In each case where this operation was performed the quantity subtracted was less than 20 per cent of the sum of the effective cross sections.

In order to derive $A_R(v',v'')$ in Eq. (27) from the Franck-Condon factors, the Einstein probabilities of spontaneous emission, $A(v',v'')$, must be expressed in terms of Franck-Condon factors. From wave mechanics,

$$A(v',v'') = \text{const.}\ \lambda_{v'v''}^{-3} \left| \int \psi_{v'} \psi_{v''} R_e dr \right|^2 \quad (26) \tag{29}$$

for diatomic molecules, where $\lambda_{v',v''}$ is a characteristic wavelength of the (v',v'') band, and $\Psi_{v'}$, $\Psi_{v''}$ are the vibrational wave functions of the upper and lower levels. R_e is the electronic transition moment given by

$$R_e = \int M_e \, \Psi_e'^* \Psi_e'' \, d\tau_e \, , \tag{30}$$

where Ψ_e' and Ψ_e'' are the molecular electronic wave functions of the upper and lower states, M_e is the dipole moment operator, and τ_e is the volume element of the space of the electronic coordinates.

If the r-centroid concept is used to account for the dependence of R_e on r, then

$$A(v',v'') = \text{const.} \; \lambda_{v',v''}^{-3} R_e^2(\overline{r}_{v',v''}) q_{v',v''}^{(27)} \tag{31}$$

where $q_{v',v''}$ is the Franck-Condon factor,

$$q_{v',v''} = \left| \int \Psi_{v'} \Psi_{v''} dr \right|^2 \, . \tag{32}$$

The r-centroid is defined as

$$\overline{r}_{v',v''} = \int \Psi_{v'} \Psi_{v''} r dr / \int \Psi_{v'} \Psi_{v''} dr \, . \tag{33}$$

Approximate values of the relative transition probabilities may be derived by assuming that $R_e(\overline{r}_{v',v''})$ is a slowly varying function of the r-centroid and is a constant for a v''-progression. Eqs. (31) and (27), then give

$$A_R(v',v'') = q_{v'v''}\lambda_{v'v''}^{-3}/\Sigma_{v''}q_{v'v''}\lambda_{v'v''}^{-3} \qquad (34)$$

Equation (34) was used to calculate the $A_R(v',v'')$ used in Eq. (28).

Apparent Cross Sections

From Eq. (10) in Chapter I, the apparent cross section of a vibrational level is given by

$$Q'(v') = \Sigma_{v''}Q(v',v'') \ , \qquad (35)$$

where the summation is over all v''. If some of the effective cross sections with the same v' have not been measured, then Q'(v') may be determined from the following equation:

$$Q'(v') = [Q(v',n) + Q(v',m) + \ldots][A_R(v',n) + A_R(v',m) + \ldots]^{-1} \qquad (36)$$

where n,m,... are the lower vibrational levels of the measured Q(v',v'') in a v''-progression with upper level v'. The apparent cross sections calculated by Eq. (36) were used in Eq. (28) to estimate the small cross sections of weak bands which overlapped strong bands in a different sequence. Table 2 lists the apparent cross sections of the vibrational levels of the $B^3\pi_g$ state calculated from Eq. (36).

Total Apparent Cross Section of the $B^3\pi_g$ State

The total apparent cross section of the $B^3\pi_g$ state as a function of the electron energy is shown in Fig. 15. The total apparent

Table 2. Apparent Electron Excitation Cross Sections of the Vibrational States of the N_2 $B^3\pi_g$ Electronic State.

v	$Q(v)(10^{-18}cm^2)$	Electron Energy (eV) At Peak
0	3.7	9.9
1	7.2	10.1
2	11.9	10.3
3	11.8	10.6
4	10.4	10.8
5	7.7	11.1
6	5.4	11.3
7	3.3	11.6
8	1.82	12.0
9	1.03	12.2
10	0.61	12.4
11	0.39	12.6
12	0.29	12.7

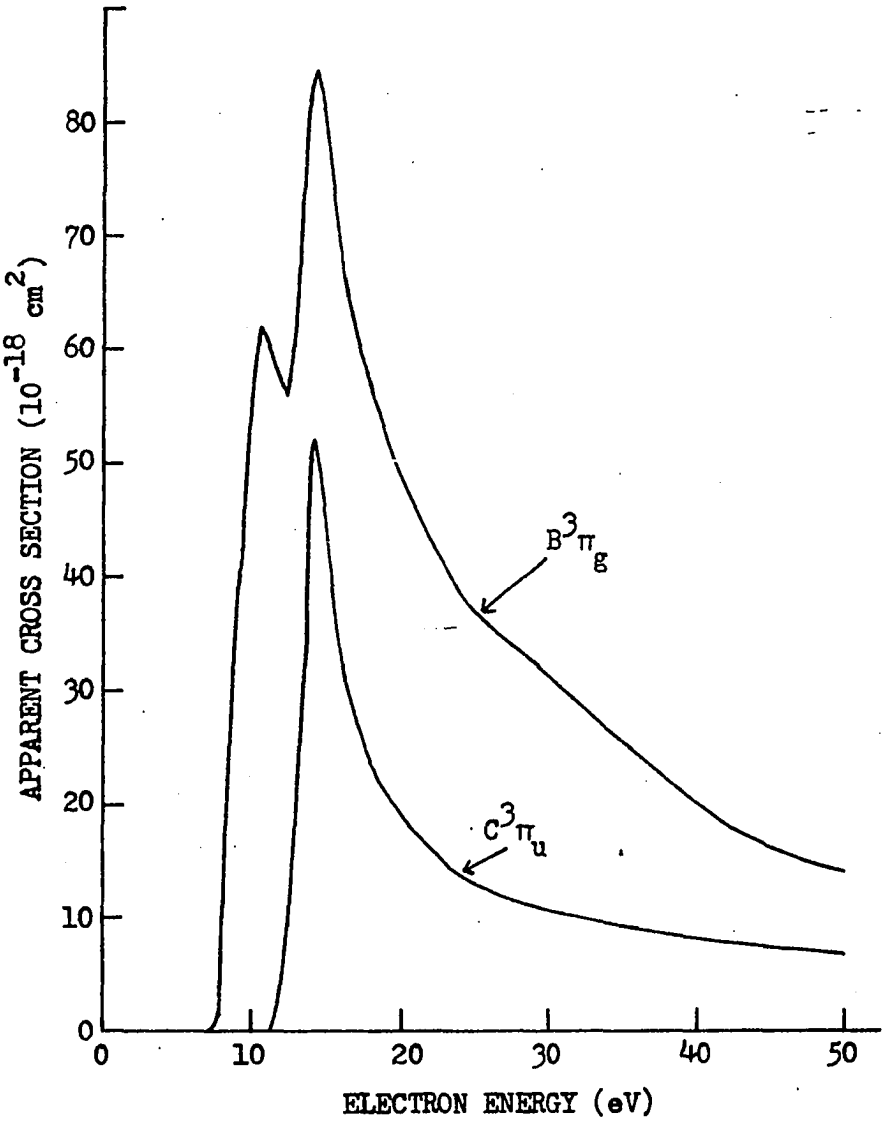

Figure 15. Apparent Excitation Cross Sections of the $B^3\pi_g$ and $C^3\pi_u$ Electronic States of N_2. (Magnitude of $C^3\pi_u$ Cross Section from Jobe, Sharpton, and St.John.[8])

cross section is the sum of the apparent cross sections Q'(v) of the vibrational levels of the $B^3\pi_g$ state. For comparison, the total apparent cross section of the $C^3\pi_u$ state (second positive system) is also shown. The magnitude of the $C^3\pi_u$ curve was taken from measurements made by Jobe, Sharpton, and St. John in the same laboratory where this experiment was conducted.[8] The apparent cross section for the $C^3\pi_u$ state gives the cascade contribution of the second positive system to the apparent cross section of the $B^3\pi_g$ state. The relative positions and heights of the two curves in Fig. 15 show that the second positive system is the major contributor to the second peak of the $B^3\pi_g$ curve and that over 50 per cent of the $B^3\pi_g$ apparent cross section at an electron energy of 14.5 eV is due to cascade from the second positive system.

Comparison of Experimental and Calculated Relative Cross Sections

The relative values of the effective cross sections Q(v',v'') in a v''-progression are determined by the relative emission transition probabilities $A_R(v',v'')$ for the progression [Eq. (28)]. Table 3 compares the variation of the approximate $A_R(v',v'')$ calculated from the Franck-Condon factors of Zare, *et al.*, using Eq. (34), with the variation of the effective cross sections Q(v',v'') in Table 1 for each v''-progression. The effective cross sections in each v''-progression were scaled by dividing them by the apparent cross section Q'(v') for the upper vibrational level of the progression taken from Table 2. The agreement between the approximate $A_R(v',v'')$ and the scaled effective

Table 3. Comparison of Relative Values of Measured Effective Cross Sections of First Positive Bands Having the Same Upper Vibrational State with the Corresponding Relative Transition Probabilities Calculated from Franck-Condon Factors.[24]
Top entry: $Q(v',v'')/Q'(v')$. Bottom entry: $A_R(v',v'')$.

v'' \ v'--	0	1	2	3	4	5	6	7	8	9	10	11	12
0	0.6	0.7	0.35	0.082		0.0012							
	0.597	0.746	0.359	0.087		0.0009							
1			0.44	0.52	0.209	0.038	0.0033						
			0.455	0.555	0.223	0.041	0.0036						
2			0.09	0.14	0.52	0.336	0.088	0.0088					
			0.071	0.150	0.551	0.360	0.090	0.0101					
3				0.19	-	0.392	0.465	0.155	0.021				
				0.147	0.014	0.428	0.459	0.155	0.022				
4					0.18	-	0.268	0.51	0.22	0.041			
					0.139	0.008	0.270	0.508	0.230	0.039			
5						0.15		0.134	0.52	0.30	0.055		
						0.086		0.134	0.505	0.307	0.063		
6										0.46	0.36	0.092	
										0.458	0.376	0.097	
7											0.41	0.44	0.131
											0.381	0.449	0.131
8												0.31	0.48
												0.299	0.481

cross section, $Q(v',v'')/Q'(v')$, was within the combined relative uncertainty of the measurements and the Franck-Condon factors for all bands except those in the $\Delta v = 0$ sequence. In the $\Delta v = 0$ sequence, the measured values were higher than the calculated values

Comparison with Other Investigators

Skubenich and Zapesochny determined the absolute apparent excitation cross section of the N_2 $B^3\pi_g$ state for electron energies up to 70 eV.[13] They used the same method that was used in this work to derive the apparent excitation cross section of the $B^3\pi_g$ state. The apparent excitation function which they published exhibits two sharp peaks at about the same electron energies as the peaks in the apparent excitation function for the $B^3\pi_g$ state shown in Fig. 15. The magnitudes of the first and second peaks in the Skubenich and Zapesochny excitation function are $100 \times 10^{-18}cm^2$ and $68 \times 10^{-18}cm^2$, compared to $62 \times 10^{-18}cm^2$ and $85 \times 10^{-18}cm^2$, respectively, found by this work. Skubenich and Zapesochny did not give a detailed explanation of their measurements of the effective cross sections of the individual bands; thus no explanation of the differences in the two apparent excitation functions can be given.

CHAPTER V

FIRST NEGATIVE AND MEINEL BAND SYSTEMS OF N_2^+

The same methods used for the study of the electron excitation of the first positive system of N_2 in Chapter IV were used to study the excitation of the first negative and Meinel band systems of N_2^+ by electron impact with N_2.

First Negative System

The first negative band system is the strongest band system of N_2^+. The upper and lower electronic states of the system, the $B^2\Sigma_u^+$ and $X^2\Sigma_g^+$ electronic states, are shown in Fig. 8. The first negative bands examined in this work extended from 3500 angstroms to 5300 angstroms, and some of them were overlapped by bands of the N_2 second positive system.

Figure 16 shows the relative excitation functions of the (0,0) and (1,0) first negative bands for electron energies up to 450 eV. The two excitation functions were identical in shape, except where the threshold of the excitation function for the (1,0) band was distorted by the overlapping (0,1) second positive band. The excitation functions exhibited broad maximums at about 120 eV and then decreased monotonically at higher energies. The effective cross section of each band at 450 eV was 66 per cent of the effective cross section at 120 eV.

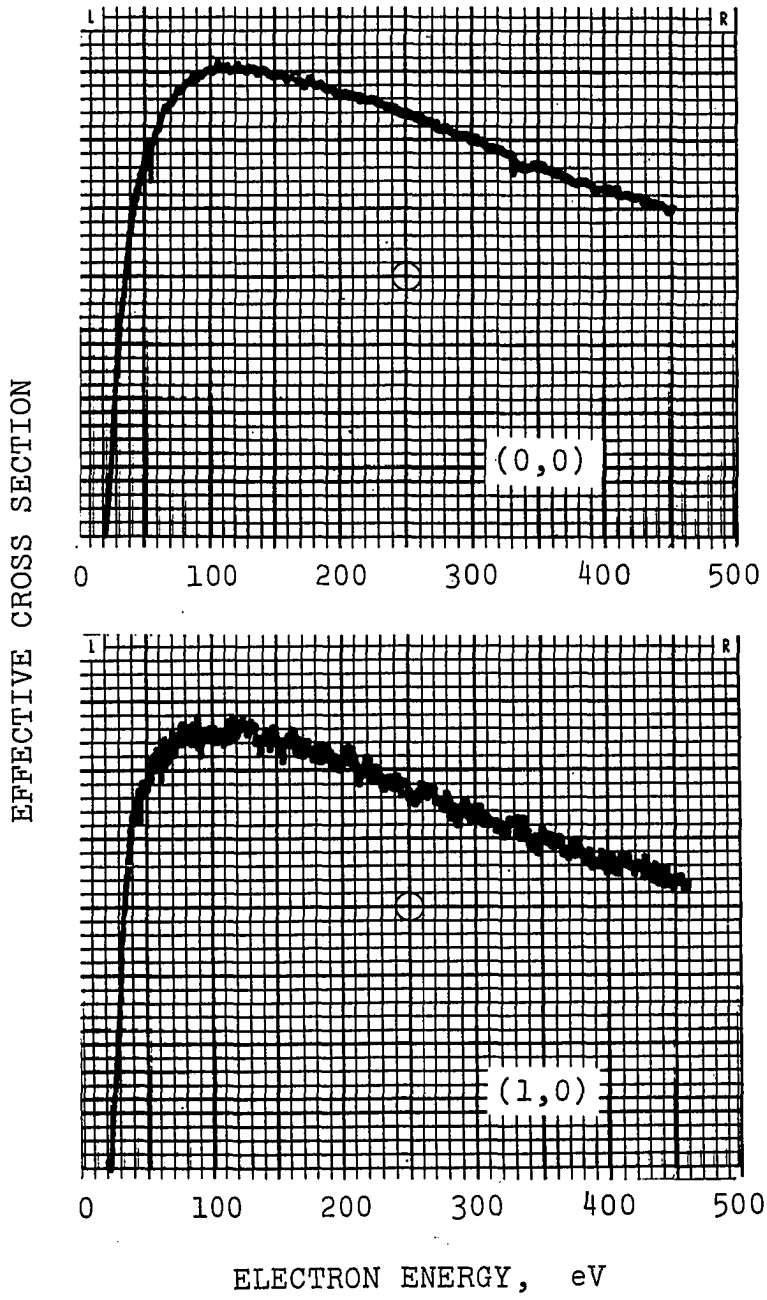

Figure 16. Relative Excitation Functions of the (0,0) and (1,0) N_2^+ First Negative Bands.

Table 4 lists the results of the measurement of the absolute effective cross section Q(v',v'') for 12 first negative bands at an electron energy of 120 eV. The estimated accuracy of the measurement for Q(0,0) is 20 per cent. The uncertainty given in Table 4 for the value of Q(0,0) is the mean deviation from the average of nine determinations of Q(0,0) at 120 eV. The uncertainties shown for the other bands in the table are estimates of the precision of their measurements.

The (1,0) first negative band of N_2^+ was overlapped by the (0,1) second positive band of N_2. To get the integrated intensity of the (1,0) band, the contribution of the second positive band was subtracted from the scan of the bands. Since the maximum of the excitation function for the second positive band lay below the onset energy of the first negative band, the contribution of the second positive band to the scan was determined by multiplying the intensity of the (0,1) second positive band at 14 eV by the ratio of the intensities of the (0,0) second positive band at 120 eV and 14 eV.

The absolute effective cross sections of the (1,0), (0,0) (0,1), (0,2), and (0,3) first negative bands in Table 4 were determined from the integrated intensities of the bands. The bands were scanned with monochromator slits just wide enough to cause blending of the rotational structure of the bands. The effective cross sections of the other bands in Table 4 were deduced by comparing the intensities of their band heads with the intensities of the (1,0), (0,0), (0,1), (0,2), and (0,3) band heads. The tail of each band that overlapped the band head of another band was extended and subtracted to get the intensity of the overlapped

Table 4. Effective Cross Sections of N_2^+ First Negative Bands at an Electron Energy of 120 eV ($10^{-18}cm^2$).

v'' \ v'--	0	1	2	3
0	15.6 ±0.6	1.00 ±.04		
1	5.4 ±.2	0.61 ±.06	0.11 ±.02	
2	1.10 ±.05	0.69 ±.05		0.050 ±.007
3	0.21 ±.01	0.27 ±.01	0.045 ±.006	
4		0.065 ±.004		

Table 5. Maximum Apparent Cross Sections of the First 4 Vibration States of the N_2^+ $B^2\Sigma_u^+$ Electronic State.

v	Q'(v) (10^{-18} cm^2)
0	22.3
1	2.6
2	0.21
3	0.09

band head. Corrections for overlapping by second positive bands were made in the same manner that corrections for the overlapping for the (1,0) band by the (0,1) second positive band were made. The intensity of the (0,0) first negative band was linear with beam current and with pressure for pressures below 5 microns. The effective cross sections in Table 4 were measured at pressures between 2 and 5 microns with a beam current of 1 ma.

The apparent cross sections Q'(v) of the first four vibrational levels of the $B^2\Sigma_u^+$ state were calculated from the measured effective cross sections of Table 4. The results are shown in Table 5. The effective cross sections in the v' = 0 and v' = 1 progressions of Table 4 were summed to get Q'(0) and Q'(1). Franck-Condon factors for the first negative system ($B^2\Sigma_u^+ - X^2\Sigma_g^+$)[28] indicated that the measured effective cross sections accounted for over 99 per cent of Q'(0) and Q'(1). Using Franck-Condon factors, Q'(2) and Q'(3) were calculated in the manner described in Chapter IV.

Figure 17 compares the experimental results of this work with the results obtained by other investigators. The effective cross sections of the (0,0) band measured by Stewart,[9] by Sheridan, *et al*,[10] and by Nishimura[11] lie below the measurements of this work by more than a factor of two. Measurements of the same cross section by McConkey, *et al.*,[12] by R. Holland[12], and by Srivastava and Mirza[14] are in excellent agreement with the present results. The maximum value of the apparent cross section of the N_2^+ $B^2\Sigma_u^+$ state, derived by summing the apparent cross sections in Table 5, agrees satisfactorily with the results

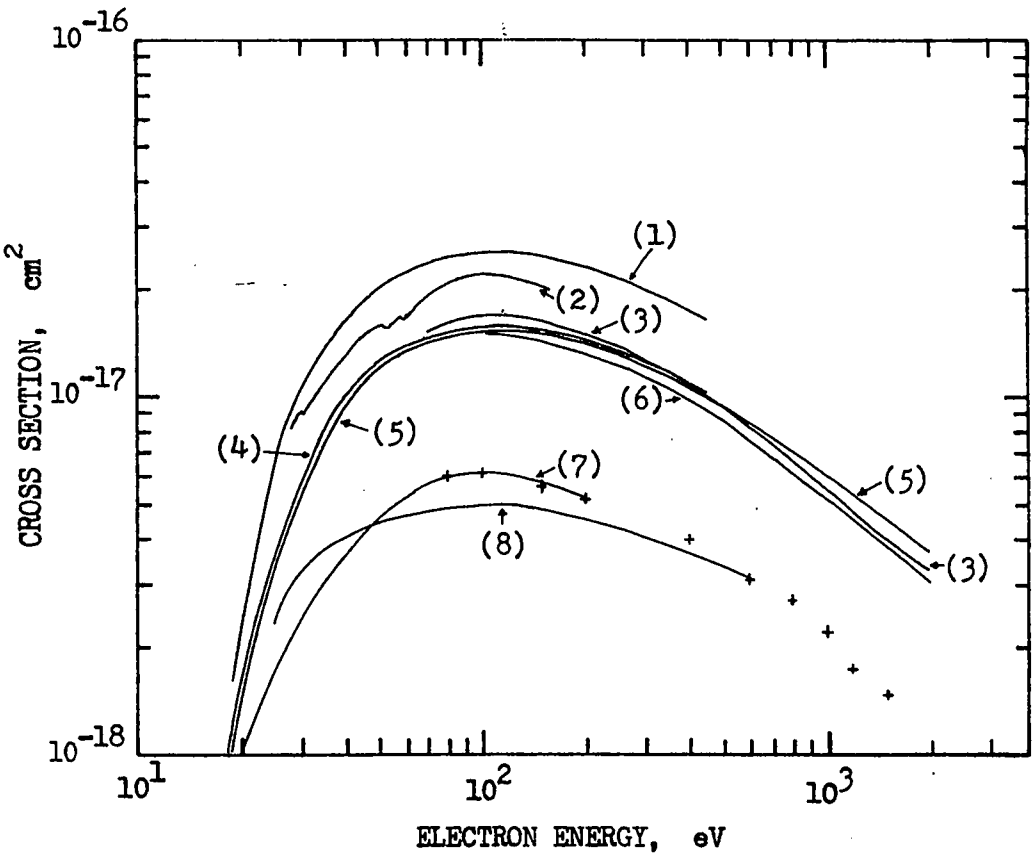

Figure 17. Apparent Cross Section of the $B^2\Sigma_u^+$ Electronic State of N_2^+:
(1) Present Results
(2) Skubenich and Zapesochny
Effective Cross Section of the (0,0) First Negative Band:
(3) Srivastava and Mirza
(4) Present Results
(5) McConkey, Woolsey, and Burns
(6) Holland
(7) Stewart
(8) Sheridan, Oldenberg, and Carleton
\+ Nishimura

obtained by Skubenich and Zapesochny.[13] Zapesochny and Kishko reported observing fine structure in the apparent excitation function of the $B^2\Sigma_u^+$ state between threshold and 80 eV;[29] however, this was not observed in the present investigation.

Meinel Band System

The Meinel band system of N_2^+ lies in the red and infrared region of the spectrum and is overlapped by the N_2 first positive system. The energy level diagram in Fig. 8 shows that N_2^+ $A^2\pi_u$ is the upper state and N_2^+ $X^2\Sigma_g^+$ is the lower state of the system. The Meinel bands are well separated from each other in the spectrum and appear as many-headed bands degraded to longer wavelengths.

Figure 18 shows the relative electron excitation functions of the (3,0) and (4,1) Meinel bands. They have broad maximums at 100 eV and then decrease monotonically at higher energies. The onset of excitation of the (3,0) Meinel band is masked by the (3,0) N_2 first positive band.

Table 6 lists the absolute effective cross sections of 10 Meinel bands at 100 eV. The cross sections were determined from the integrated intensities of the bands. The overlapping first positive bands were subtracted from the scan of the Meinel bands. Since the onset energies of the Meinel bands lay at electron energies above the maxima of the excitation functions of the first positive bands, the amount to subtract was determined by comparing the scan of the spectrum at low electron energy to the scan at 100 eV.

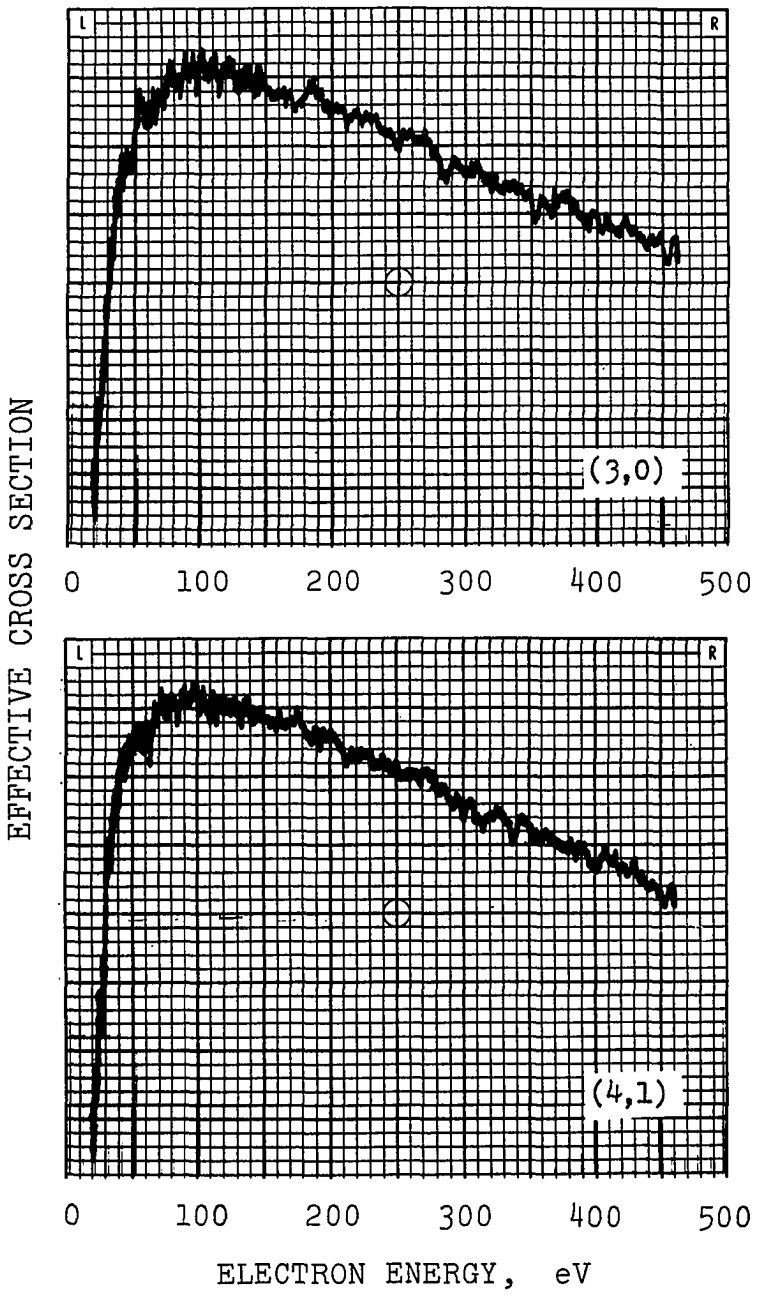

Figure 18. Relative Excitation Functions of the (3,0) and (4,1) N_2^+ Meinel Bands.

Table 6. Effective Cross Sections of N_2^+ Meinel Bands at 100 eV (10^{-18} cm^2).

v'-- 0 / v''	1	2	3	4	5
0	8 ±1	11 ±1	4.5 ±.2	1.22 ±.05	0.24 ±.01	
1			5.8 ±.6	2.93 ±.15	1.03 ±.04	0.27 ±.01
2						0.59 ±.06

Table 7. Maximum Cross Sections of the First 6 Vibrational States of the N_2^+ $A^2\pi_u$ Electronic State at 100 eV.

v	Q(v) (10^{-18} cm^2)
0	11
1	15
2	11.5
3	5.6
4	2.7
5	1.3

The error limits given for the measurements in Table 6 are an estimate of the uncertainty of the relative measurements within the Meinel system. The absolute accuracy of the cross section measurements is estimated to be 20 per cent.

Table 7 gives the apparent electron excitation cross sections of the vibrational levels, v' = 0 - 5, of the $N_2^+ A^2\pi_u$ state at 100 eV. Franck-Condon factors for the ($A^2\pi_u$ - $X^2\Sigma_g^+$) Meinel band system[28] were used to calculate the apparent cross sections for each v' from the effective cross sections with upper level v' in Table 6. The sum of the apparent cross sections in Table 7 gives the value of 47 x 10^{-18} cm^2 for the total apparent cross section for the electron excitation of the first six vibrational levels of the $N_2^+ A^2\pi_u$ state at 100 eV. This value agrees closely with the value of 46 x 10^{-18} cm^2 for the apparent cross section of the $N_2^+ A^2\pi_u$ state at 100 eV read from the absolute excitation function reported by Skubenich and Zapesochny.[13] The maximum of their excitation function, however, was 57 x 10^{-18} cm^2 at 62 eV.

CHAPTER VI

CONCLUSION

The experimental apparatus and techniques for measuring electron excitation cross sections of molecular nitrogen using an optical method have been described, and results of measurements in the N_2 first positive, N_2^+ first negative, and N_2^+ Meinel band systems have been given.

Relative effective excitation functions from 0 - 50 eV were presented for first positive ($B^3\pi_g$ - $A^3\Sigma_u^+$) bands with upper vibrational states v' = 0 through 9. The first positive bands with v' = 10, 11, and 12 were either too weak or were too severely overlapped by radiation from other spectral features to obtain their excitation functions to 50 eV. The excitation functions exhibited two sharp peaks at 10 - 12 eV and at 14 - 15 eV. At 50 eV the excitation functions were less than 20 per cent of their maximum values at lower energies.

The second peak in the excitation function of a first positive band was primarily caused by cascade from the second positive system. Decreasing contribution of the second positive cascade caused the magnitude of the second peak to decrease in relation to the height of the first peak as v' increased. The relative heights of the peaks in the excitation function for the (0,0) band indicated that almost 90 per cent of the excitation of the (0,0) band at 14.2 eV was from cascade.

The threshold of the relative electron excitation functions of 11 first positive bands with v' = 2 through 12 were shown with an expanded energy scale. The expansion of the energy scale revealed that the first positive excitation functions exhibited a decrease in slope followed by an increase in slope about midway between onset and the maximum of the first sharp peak.

Absolute effective excitation cross sections were listed for 39 first positive bands at the electron energy of the maximum in the first sharp peak of the excitation functions. The relative values of the effective cross sections in each v''-progression were compared with relative transition probabilities calculated from Franck-Condon factors for the $B^3\pi_g$ - $A^3\Sigma_u^+$ transitions. There was agreement within the uncertainty of the numbers compared for all bands but those of the $\Delta v = 0$ sequence. Also listed were apparent excitation cross sections calculated for the v = 0 through 12 vibrational states of the $B^3\pi_g$ electronic state from the effective cross sections of the first positive bands.

The apparent cross sections for the vibrational levels of the $B^3\pi_g$ state were summed to get the apparent excitation function for the $B^3\pi_g$ state. This excitation function and the one reported by Skubenich and Zapesochny[13] exhibited several differences in both magnitude and shape. It is suggested that perhaps Skubenich and Zapesochny relied too heavily on Franck-Condon factors in determining their curve and did not measure the absolute effective cross sections and excitation functions of as many bands as this work.

The absolute effective excitation cross sections of 12 N_2^+ first negative bands at 120 eV were listed, and relative excitation functions from 0 to 450 eV for the (0,0) and (1,0) bands were given. The excitation functions peaked at 120 eV and decreased slowly at higher energies. Apparent cross sections at 120 eV for the first four vibrational states of the N_2^+ $B^2\Sigma_u^+$ state were calculated using the Franck-Condon factors for the N_2^+ first negative ($B^2\Sigma_u^+ - X^2\Sigma_g^+$) system.

The absolute effective excitation function of the (0,0) first negative band determined by this work was compared with similar curves obtained by previous investigators. The results of this work agreed closely with the measurements of McConkey, *et al.*,[12] of Holland,[12] and of Srivastava and Mirza[14]. However, the excitation functions for the (0,0) first negative band reported by Stewart,[9] by Sheridan *et al.*,[10] and by Nishimura[11] were all lower than the curve given in the present work by about a factor of two. The maximum of the total apparent cross section for the excitation of the first four vibrational states of the N_2 $B^2\Sigma_u^+$ state in this work (25×10^{-18} cm^2) agreed satisfactorily with the maximum apparent cross section for the $B^2\Sigma_u^+$ state from the investigation by Skubenich and Zapesochny (22×10^{-18} cm^2).[13]

In addition to the measurements made in the N_2^+ first negative system, N_2^+ Meinel bands ($A^2\pi_u - X^2\Sigma_g^+$) were investigated. Relative excitation functions for the (3,0) and (4,1) Meinel bands were given, and the excitation functions for both bands were found to have identical shapes. Absolute effective excitation cross sections were measured for

10 Meinel bands at 100 eV, the position of the maximum in the excitation functions. Apparent excitation cross sections for the first six vibrational states of the N_2^+ $A^2\pi_u$ state at 100 eV were calculated, and their sum agreed in magnitude with the value of the apparent cross section of the $A^2\pi_u$ state at 100 eV derived from the excitation function reported by Skubenich and Zapesochny.[13] However, the excitation function of these investigators peaked at about 62 eV rather than at 100 eV as reported by this work.

The absolute effective electron excitation cross sections of a total of 61 bands of N_2 and N_2^+ were measured under conditions of low pressure and low beam current. The estimated accuracy of the measurements ranged from 20 per cent to 40 per cent. The less accurate measurements resulted from difficulty in determining the integrated intensity of bands that were severely overlapped by other bands or that were hard to detect because of their wavelength or their strength.

LIST OF REFERENCES

1. D. C. Duncan, Astrophys. J. 62, 145 (1925).
2. G. O. Langstroth, Proc. Roy. Soc. (London) A146, 167 (1934).
3. S. E. Williams, Proc. Phys. Soc. (London) A47, 420 (1935).
4. F. P. Bundy, Phys. Rev. A52, 698 (1937).
5. D. T. Stewart, Proc. Phys. Soc. (London) A68, 404 (1955).
6. D. T. Stewart and E. Gabathuler, Proc. Phys. Soc. (London) A72, 287 (1958).
7. Von E. Fink and K. H. Welge, Zs. Naturforsch. 19a, 1193 (1964).
8. John D. Jobe, Francis A. Sharpton, and R. M. St. John, J. Opt. Soc. Am. 57, 106 (1967).
9. D. T. Stewart, Proc. Roy. Soc. (London) A69, 437 (1956).
10. W. F. Sheridan, O. Oldenberg, and N. P. Carleton, Abstr. II Int. Conf. Phys. Electronic and Atomic Collisions (New York: W. A. Benjamin, Inc., 1961), p. 159.
11. Hiroyuki Nishimura, J. Phys. Soc. Japan 24, 130 (1968).
12. J. W. McConkey, J. M. Woolsey, and D. J. Burns, Planet. Space Sci. 15, 1332 (1967).
13. V. V. Skubenich and I. P. Zapesochny, Abstr. V. Int. Conf. Phys. Electronic and Atomic Collisions (Leningrad: Publishing House <<Nauka>>, 1967), p. 570.
14. B. N. Srivastava and I. M. Mirza, Phys. Rev. 168, 86 (1968).
15. Gerhard Herzberg, Molecular Spectra and Molecular Structure: I. Spectra of Diatomic Molecules (New York: D. Van Nostrand Company, Inc., 1950), p. 123.

16. A. E. de Vries and P. K. Pol, Vacuum 15, 135 (1965).

17. John T. Merrill and R. Gray Layton, Appl. Opt. 5, 1818 (1966).

18. J. C. DeVos, Physica 20, 690 (1954).

19. John D. Jobe, Ph.D. Dissertation, "Excitation Processes in Helium", University of Oklahoma. Norman, Oklahoma (1968), p. 15.

20. Varian Vacuum Views (Palo Alto, California: Varian, 1967), p. 2.

21. R.W.B. Pearse and A. G. Gaydon, The Identification of Molecular Spectra, 3rd ed. (London: Chapman and Hall, 1963), p. 210.

22. M. Jeunehomme, J. Chem. Phys., (U.S.A.) 45, 1805 (1966).

23. M. Jeunehomme, J. Chem. Phys. (U.S.A.) 44, 2672 (1966).

24. William Benesch and Joseph T. Vanderslice, S. G. Tilford and P. G. Wilkinson, Astrophys. J. 142, 1227 (1965).

25. R. N. Zare, E. O. Larrson, and R. A. Berg, J. Mol. Spectrosc. 15, 117 (1965).

26. Gerhard Herzberg, Spectra of Diatomic Molecules, p. 20 and p. 200.

27. R. W. Nicholls and W. R. Jarmain, Proc. Phys. Soc. A69, 253 (1956).

28. R. W. Nicholls, J. Res. Natl. Bur. Std. A65, 451 (1961).

29. I. P. Zapesochny and S. M. Kishko, Soviet Phys. - Doklady 5, 1008 (1961).